AVOIDING EARTH IMPACTS USING ALBEDO MODIFICATION AS APPLIED TO 99942 APOPHIS

A Thesis

by

RICHARD STEVEN MARGULIEUX

Submitted to the Office of Graduate Studies of
Texas A&M University
in partial fulfillment of the requirements for the degree of

MASTER OF SCIENCE

May 2010

Major Subject: Aerospace Engineering

AVOIDING EARTH IMPACTS USING ALBEDO MODIFICATION AS APPLIED TO 99942 APOPHIS

A Thesis

by

RICHARD STEVEN MARGULIEUX

Submitted to the Office of Graduate Studies of
Texas A&M University
in partial fulfillment of the requirements for the degree of

MASTER OF SCIENCE

Approved by:

Chair of Committee,	David Hyland
Committee Members,	John Hurtado
	Mark Lemmon
Head of Department,	Dimitris Lagoudas

May 2010

Major Subject: Aerospace Engineering

ABSTRACT

Avoiding Earth Impacts Using Albedo Modification as Applied to 99942 Apophis. (May 2010)
Richard Steven Margulieux, B.S., Texas A&M University
Chair of Advisory Committee: Dr. David Hyland

Current orbital solutions for 99942 Apophis predict a close approach to the Earth in April 2029. The parameters of that approach affect the future trajectory of Apophis, potentially leading to an impact in 2036, 2056, 2068, etc. The dynamic model used for this prediction does not account for non-gravitational perturbations including solar pressure and the Yarkovsky effect. Estimates of the displacement due to these perturbations range from -1500 to 1500km by 2029, comparable to 7σ uncertainty in orbital solution. Uncertainties in physical characteristics stem from a lack of direct observations and a shortage of empirical data on similar objects. These perturbations, which stem from interactions with solar radiation, are directly related to the albedo of Apophis' surface. By modifying the average albedo of Apophis by 0.5%, between 4 and 15m of displacement can be effected between 2023 and 2029, rendering this method capable of avoiding all near-nominal solution keyholes. This modification is obtained by the deposition of electrostatically charged particles. These particles are charged via tribo-electrification and cure on the surface of Apophis creating a 30 micron thick layer of material with desired properties. This study found that a change in average albedo would nominally require 160kg of polytetrafluoroethylene (PTFE) to increase by 0.5% or 290kg of PTFE to decrease by 0.5%. The Apophis Exploration and Mitigation mission concept both improves accuracy of non-

gravitational perturbation models and delivers the albedo modification mechanism to Apophis, launching in 2021 and modifying albedo in 2023.

ACKNOWLEDGEMENTS

The author thanks Dr. David Hyland, Dr. John Hurtado, and Dr. Mark Lemmon for reviewing this thesis. I would like to acknowledge the Texas A&M University Apophis Study Group for ideas and research related to the asteroid 99942 Apophis. The modification technique discussed in this thesis was developed by the group over the past year. Additional thanks goes to NASA-Ames Research Center: Mission Design Center, for helping myself and the group to develop the Apophis Exploration and Mitigation Platform mission concept. I would also like to acknowledge Jon Giorgini, whose paper "Predicting Earth encounters of Apophis" mentions the idea of modifying albedo to alter Apophis' trajectory. I would like to thank Steve Chesley for his correspondence regarding Apophis trajectory and keyhole locations.

TABLE OF CONTENTS

LIST OF FIGURES

Page

Page

LIST OF TABLES

Page

I. INTRODUCTION

A survey of the crust of the Earth reveals numerous impact craters such as Barringer's Crater in Arizona (Barringer, 1905) and Upheaval Dome in Utah (Kriens et al, 1999). The fossil record has shown that history of life on Earth is punctuated with mass extinction events coinciding with major impacts (Alvarez et al, 1980). The conglomerated remnants of the solar systems formation, asteroids and comets pose a potential threat to life on Earth. In recent years, the number of known small solar system bodies has grown with mankind's increasing vigilance towards the heavens.

Of particular interest are small bodies with Earth crossing orbits called near-Earth objects (NEOs). NEOs are commonly defined as asteroids and comets with perihelion distances, q, less than 1.3 AU. They can be further classified as Atens, with semi-major axes, a, less than the Earth's 1.0 AU and aphelion distances, Q, greater than 0.983 AU; Apollos, with $a \geq 1.0$ AU and $q \leq 1.0167$ AU; or Amors, with $1.0167 \leq q \leq 1.3$ AU (Morbidelli, 2002). Asteroids larger than 150m diameter and deemed to have a Minimum Orbit Intersection Distance (MOID) less than 0.05 AU with the Earth are further labeled potential hazardous asteroids (PHAs) (JPL Near Earth Object Program, 2010). Morbidelli estimates only 1% of NEOs ultimately impact the Earth, with the remainder being swallowed by the sun or ejected from the inner solar system after interactions with Jupiter.

This thesis follows the style of the *AIAA Journal*.

Starting in the late 1990's NASA was tasked by congress to coordinate a search program that would discover 90% of all NEOs 1km or larger within 10 years. As of January 18, 2010, the program has discovered 6684 NEOs, with approximately 1086 of these NEOs 1km in diameter or larger. 1094 objects are further classified as PHAs (JPL/NEO). Using results from this search, Stuart (2001) predicts the NEO population sized larger than 150m will eventually found to be near 100,000 with 1200±100 larger than 1km.

In 2005, the Hayabusa spacecraft undertook a period of proximity operations about the asteroid Itokawa, a sub-km class NEO. The high-resolution imagery, see Figure 1, and property measurements taken during this period have greatly expanded our understanding of NEOs (JAXA).

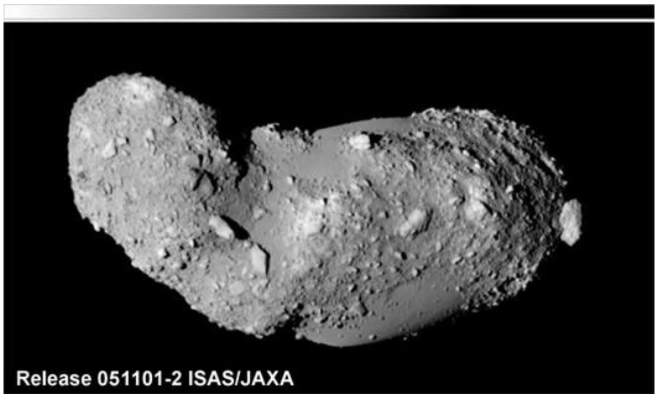

Fig. 1 Asteroid Itokawa (JAXA)

The body of this thesis will focus on the NEO 99942 Apophis discovered in June 2004 at Kitt Peak. By December of that year, Chesley reported a 2.7% impact probability for 2029 (Yeomans et al, 2004). Further measurements through 2006 brought the impact probability in 2029 to zero. However for reasons discussed in the next section, despite the trajectory being projected to narrowly miss the Earth in 2029, the resulting trajectory from the close approach may result in a future impact in 2036, 2037, 2068, etc (Chesley, 2009).

The thesis will review the process of predicting impacts and show the current situation for Apophis. Next, the author will show the development of non-gravitational perturbation models. After a review of the current estimates for Apophis' physical properties, Apophis' orbit will be propagated while accounting for these perturbations. Furthermore, a novel concept developed at Texas A&M University to modify NEO orbits using albedo modification is discussed. Finally, the effectiveness of this concept is tested against the probable cases presented by Apophis.

II. UNDERSTANDING THE NEO PROBLEM

Near Earth Objects encompass a broad range of solar system bodies: from dust particles to km class objects; from comets to rubble-piles to past main-belt objects. Aten's, like Apophis, orbit in proximity with the Earth for millions of years before undergoing a major trajectory alteration or impacting the Earth (Morbidelli, 2002). During this period, the NEOs interact with the Earth and other bodies, and are subject to non-gravitational perturbations. To understand the threat from NEOs, it is important to look in the near- and long-term.

Apophis' orbit

Due to its threatening nature, much effort has been spent determining the orbit of 99942 Apophis. Giorgini, et al (2008) detail a solution based upon measurements taken through May 2006 and, Chesley et al (2009) refines that solution with additional measurements from January 2008. The results of Chesley's latest orbit determination with the associated uncertainty are displayed in Table 1 (JPL Small-Body Database).

Table 1
Orbital Elements of 99942 Apophis (heliocentric elliptic J2000) (JPL)

Element	Value	Uncertainty (1σ)	Unit
Eccentricity (e)	0.191211060480	3.6282e-08	
Semi-major axis (a)	0.9224192977379	7.8358e-09	AU
Inclination (i)	3.3315177800	1.5068e-06	deg
Longitude of the ascending node (Ω)	204.439303961	3.0199e-05	deg
Argument of the perihelion (ω)	126.424470530	3.0823e-05	deg
Time of perihelion passage (t_p)	2455218.523239658	2.0591e-05	JED
Period (P)	323.5869489330	4.1233e-06	d
Mean motion (n)	1.112529418096	1.4176e-08	deg/d
Perihelion distance (q)	0.746042525610	3.8967e-08	AU
Aphelion distance (Q)	1.0987960698660	9.3341e-09	AU

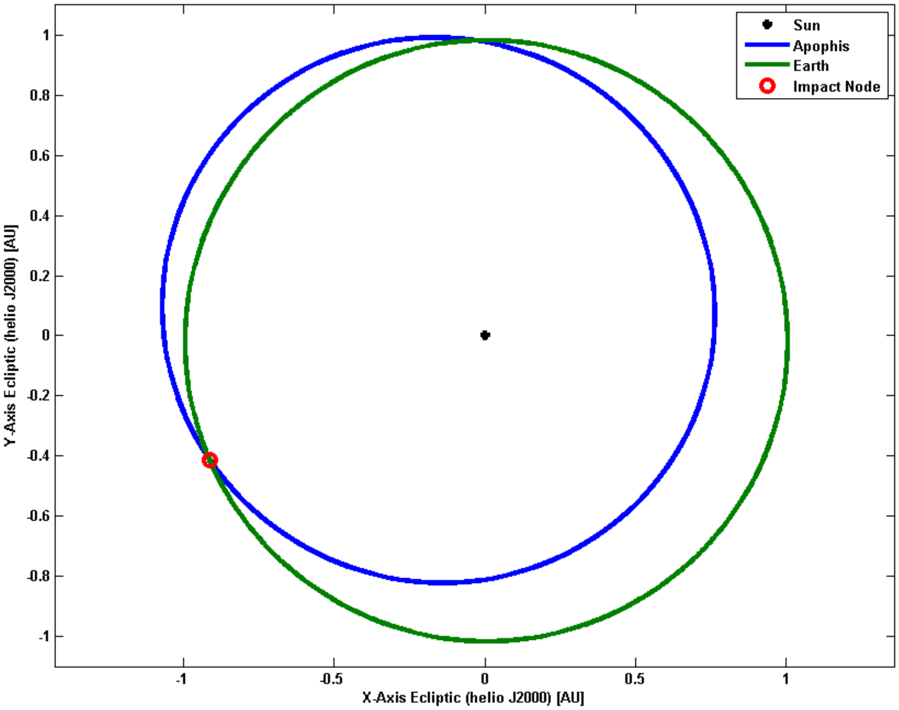

Fig. 2 Apophis and Earth orbits: on the ecliptic plane

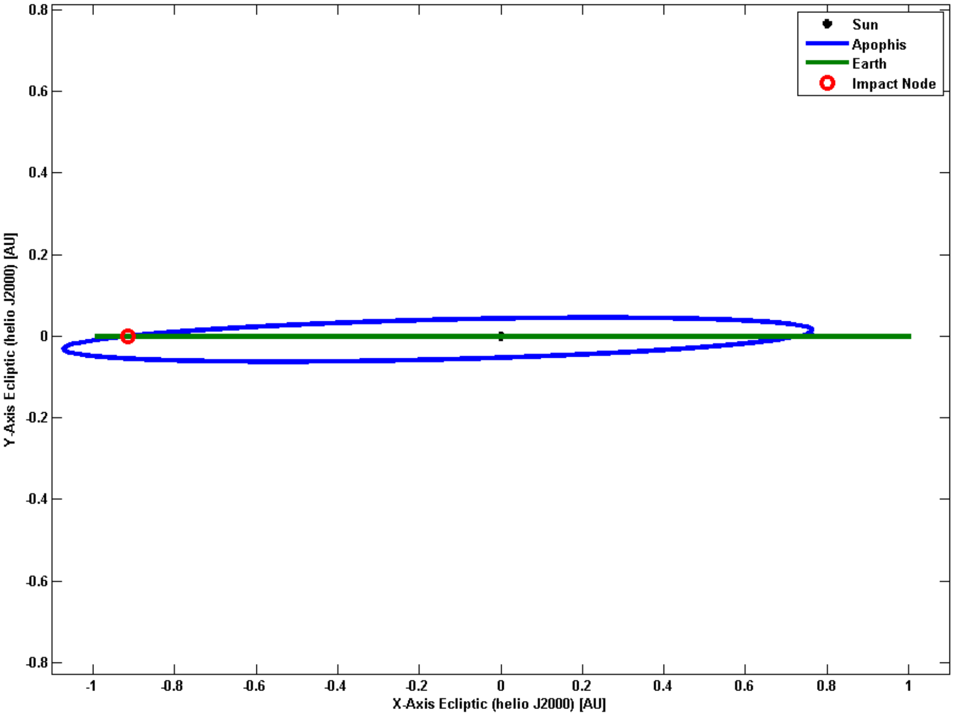

Fig. 3 Apophis and Earth orbits: edge-on view

This orbit solution is based upon 640 observations, including 2 radar delay observations and 5 radar Doppler observations, over a data-arc span of 1395 days between March 15, 2004 and January 9, 2008. Figures 2 and 3 show the relation between Apophis' and Earth's orbits. Earth's orbital elements are gathered from (JPL Horizons) for April 13th, 2029 and are included in Appendix A.

Impact node and perturbations

(Giorgini, 2008) backward and forward propagates Apophis' trajectory to show a history of close approaches (CA) with the Earth. While Apophis has approached within 0.1 AU of the Earth ten times and Venus eight times between April 1869 and December 2004, Table 2 is reduced to include only close approaches within 0.05 AU of the Earth. The minimal orbit intersection lies at the impact node, in the vicinity of April 13th with a distance of 0.00003187 AU or 4768 km or 0.7476 R_e (JPL Small Body Database). Furthermore, Apophis is shown to currently approach Earth approximately every 8 years after having completed 9 of its own orbits. Figure 4 demonstrates the resonant nature of Apophis' and Earth's orbits.

Table 2
Close Approaches (<0.05 AU) with the Earth (Giorgini, 2008)

Date	CA Distance (AU)	Vrel (km/s)	CA Time Uncertainty (3σ) (min)
1907 Apr 13.14345	0.027612	5.123	383.44
1949 Apr 14.47917	0.027916	6.689	0.16
1990 Apr 14.86420	0.032939	6.845	0.07
1998 Apr 14.82361	0.024385	6.585	0.07
2029 Apr 13.90711	0.000254	7.422	0.66

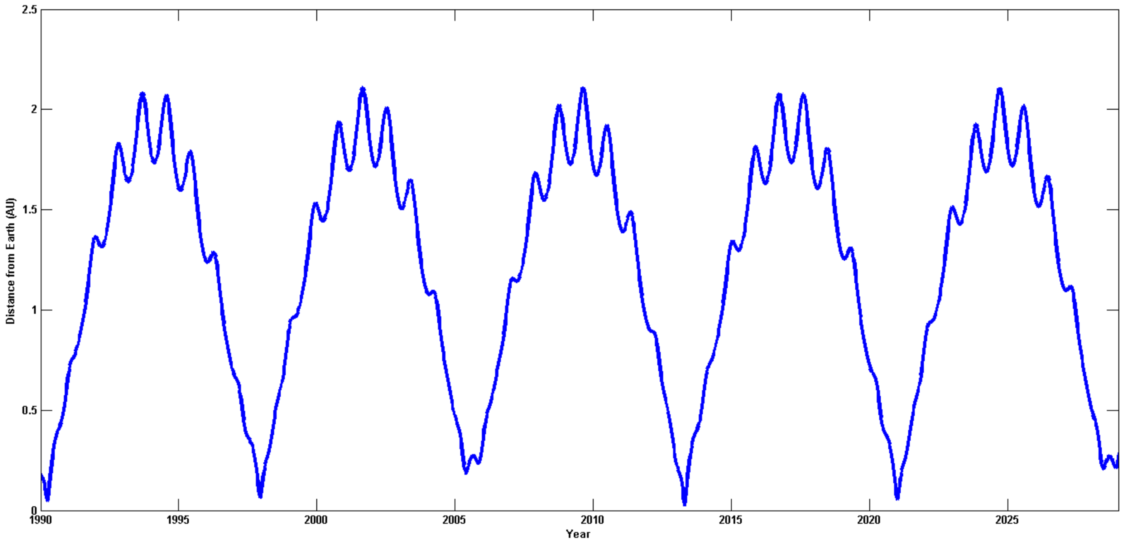

Fig. 4 Distance between Apophis and Earth (1990-2029)

Obviously this demonstrates that if both orbits were unperturbed ad infinitum, an impact would be inevitable. However, Apophis' orbit is perturbed regularly by many gravitational sources, and a few non-gravitational sources. (Giorgini, 2008) explains that "the Standard Dynamical Model (SDM), used for all asteroid solutions and propagations, includes n-body relativistic gravitational forces caused by the Sun, planets, Moon, Ceres, Palas, and Vesta," and further states that some perturbations are un-modeled such as asteroid-asteroid interactions, thermal radiation, and solar pressure. For the purposes of this thesis, only close encounters with the Earth, and absorptive-emissive phenomena related to solar radiation will be accounted for when propagating Apophis' trajectory with reliance on previously calculated (see Giorgini, 2008 and Chesley, 2009) solutions when available.

Close approaches, resonance, and keyholes

While most of these perturbations have minor effect on Apophis' trajectory, only periodic close approaches with the Earth, moon, and Venus produce significant, episodic alterations to Apophis' orbit. As Morbidelli (2002) states in "Origin and Evolution of NEOs" "asteroids become planet crossers by increasing their eccentricity under the action of resonant phenomena." Resonant phenomena being the periodic perturbations near the same position in the orbit, in his context, main-belt objects interacting with Jupiter. Similarly, interactions between Apophis and Earth, which presently have a 9:8 resonance structure, will produce major alterations to Apophis' orbit.

The 2029 close approach is the manifestation of this resonance phenomenon. As Apophis, passes within 0.00027 AU (40000km) of the Earth in a hyperbolic orbit, the perturbation on Apophis' orbit will create a significantly altered trajectory. Due to the uncertainty in Apophis' current orbit solution, the exact distance of the close approach is only known to 0.00002 AU (30000km) or one order of magnitude less than the close approach distance itself. Therefore a whole range of possible post-CA orbits exist, see Figure 5, all varying significantly depending on the initial conditions of the orbit. Because the orbit perturbation occurs at the impact node, the impact node will not shift significantly, only the ratio of the resonance.

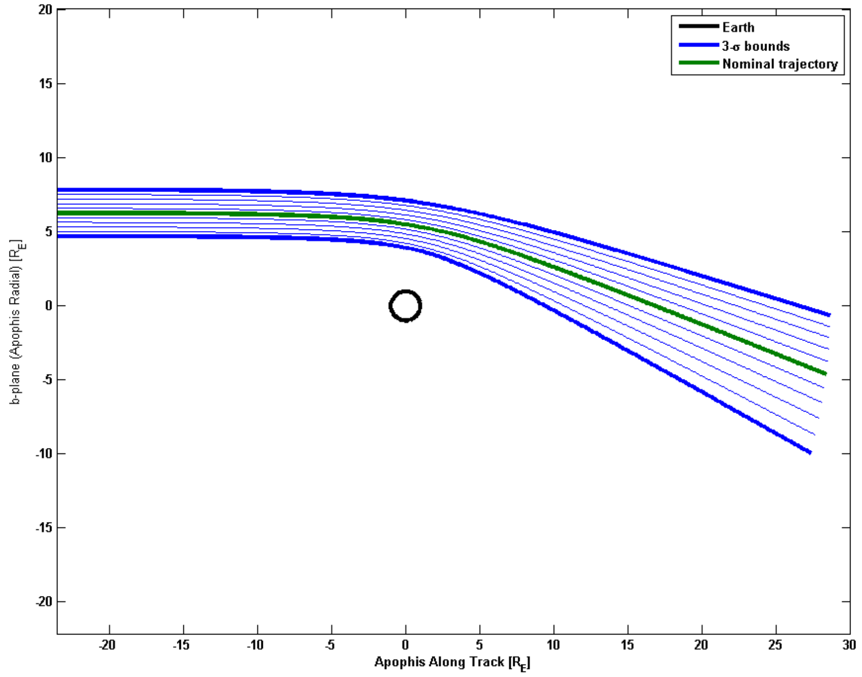

Fig. 5 Possible trajectories within 3-sigma bounds of uncertainty during 2029 CA

The most threatening outcomes from the 2029 close approach are called “resonant returns.” Where as the current resonance structure is 9:8, any post-CA orbit that produces a resonant structure relative to Earth is just as hazardous as the pre-2029 orbit. Furthermore, if the pre-2029 trajectory passes through a “keyhole,” an exact resonant return will occur and Apophis will impact the Earth. Therefore, the remainder of this section will be dedicated to finding keyholes existing in the region of possible orbit solutions.

Opïk’s theory of close encounters, the b-plane, and Valsecchi circles

Opïk’s (1976) theory of close encounters models the trajectory of a small body approaching the Earth as a Keplerian, geocentric, hyperbolic orbit. The relative velocity of the asteroid with respect to the Earth defines the initial asymptote; the encounter effecting an instantaneous deflection on the velocity of the asteroid and generating the final asymptote. Opïk’s theory assumes Earth to have an exactly circular orbit, and neglects perturbations due to the Sun’s gravitation during the CA event. The velocity vector is approximated as a function of the semimajor axis, eccentricity, and inclination. Errors in this approach decrease with the minimum approach distance, and vanish as this approach distance goes to zero.

Consider an asteroid encountering the Earth, which has a circular orbit about the Sun. Following (Carusi, 1990), we scale the distance between the Earth and the Sun to 1, set the Sun’s gravitational parameter to unity, which rescales the period to 2π. We first create a geocentric reference frame (X, Y, Z) such that the Y-axis is coincident with the velocity vector of the Earth, the X-axis is the radial vector from the Sun, and the Z-axis completes a right-handed coordinate system. The components of the asteroid’s geocentric velocity vector, **U**, are given as

$$\begin{bmatrix} U_x \\ U_y \\ U_z \end{bmatrix} = \begin{bmatrix} \pm\sqrt{2 - \frac{1}{a} - a(1-e^2)} \\ \sqrt{a(1-e^2)}\cos i - 1 \\ \pm\sqrt{a(1-e^2)}\sin i \end{bmatrix} \tag{1}$$

with the geocentric speed of the asteroid being

$$U = \sqrt{3 - T} \tag{2}$$

where T is the Tisserand parameter with respect to the Earth.

$$T = \frac{1}{a} + 2\sqrt{a(1-e^2)}\cos i \tag{3}$$

Next, we define a second reference frame based upon the b-plane. The b-plane lies orthogonal to the asteroid’s velocity, **U**, containing the center of the Earth. The **b** vector, lies on the b-plane and extends from Earth’s center to the asteroid’s initial asymptote. The magnitude of the **b** vector is often referred to as the impact parameter. The b-plane frame, see Figure 6, uses the coordinate system (ξ, ς, η), where (ξ, ς) are coordinates of the b-plane, and η-axis coincides with the **U** vector. The ς-axis lies opposite the Earth's velocity vector as it is projected onto the b-plane. The ξ-axis completes a right-handed coordinate system. Because the ξ-axis is orthogonal to both the Earth's and asteroid's velocities, the MOID lies on this axis. Conversely, the ς-axis represents possible positions of the Earth dependant on time. Therefore, the two coordinates decouple into distance between the orbits, ξ, and timing of the encounter, ς.

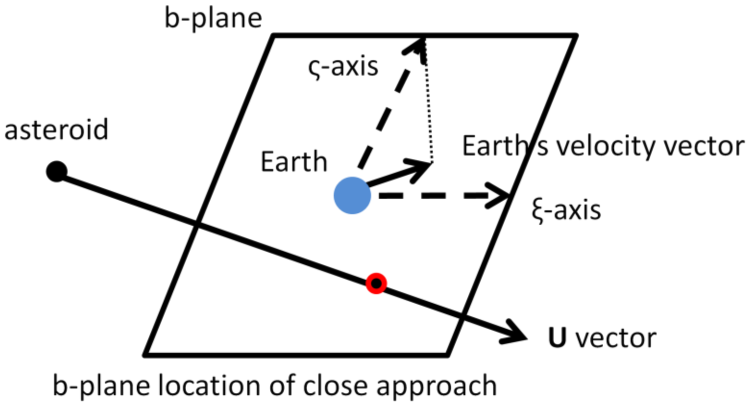

Fig. 6 b-plane coordinate system

The relationship between these two frames is given by

$$\begin{bmatrix} \xi \\ \eta \\ \varsigma \end{bmatrix} = C_\xi(-\theta)C_Y(-\phi)\begin{bmatrix} X \\ Y \\ Z \end{bmatrix} \tag{4}$$

where $C_\xi(\theta)$ represents a rotation of θ about the ξ-axis, and the angles, ϕ and θ relate the two orbits. The values for these angles are given as

$$\theta = \cos^{-1}\frac{U_y}{U} \tag{5}$$

and

$$\phi = \tan^{-1}\frac{U_x}{U_z} \tag{6}$$

The encounter with the Earth rotates **U** into **U**’ with the following relationship from (Valsecchi, et al 2003)

$$\cos\theta' = \cos\theta\cos\gamma + \sin\theta\sin\gamma\cos\psi \qquad (7)$$

and

$$\tan(\phi - \phi') = \frac{\sin\psi\sin\gamma}{\sin\theta\cos\gamma - \cos\theta\sin\gamma\cos\psi} \qquad (8)$$

where γ is the deflection of the orbit tangent and ψ is the angle about the η-axis on the b-plane. These angles are calculated by

$$\gamma = 2\tan^{-1}\frac{m}{bU^2} \qquad (9)$$

where m is the mass of the Earth, and

$$\psi = \cos^{-1}\frac{\varsigma}{\mathrm{b}} \qquad (10)$$

Since Earth’s orbital period is set to 2π, and the new orbital period of the asteroid is $2\pi a`^{3/2}$, the objects will be in the proximity of the impact node coincidentally if $a'^{3/2}=k/h$, where k and h are integers. After k years, and h periods of the asteroid have transpired, a resonant return will take place and another encounter will take place. If this ratio is inexact, the position in η will vary. The time of the second encounter can be calculated using

$$t'' = t' + 2\pi h a'^{3/2} \qquad (11)$$

To solve for all possible resonant returns with values of k and h, we solve for a specific final semimajor axis, a’

$$a' = \sqrt[3]{\left(\frac{k}{h}\right)^2} \tag{12}$$

Valsecchi shows that for each a’, there exist a circle of possible trajectories on the b-plane that would yield a’. This circle is described as

$$\xi + \varsigma - 2D\varsigma + D^2 = R^2 \tag{13}$$

where R is the radius of the circle, and D is the ς value of the center. The values are

$$R = \left|\frac{m \sin\theta'}{U^2(\cos\theta' - \cos\theta)}\right| \tag{14}$$

and

$$D = \frac{m \sin\theta'}{U^2(\cos\theta' - \cos\theta)} \tag{15}$$

where

$$\theta' = \cos^{-1}\frac{1 - U^2 - \frac{1}{a'}}{2U} \tag{16}$$

Valsecchi circles define a region of keyholes. The “line” of the circle denotes the keyhole locations, and the width of the line depends upon the CA parameters. In general, the nearer term the predicted impact, the thicker the keyhole. The Valsecchi circle line represents a direct strike in the center of the Earth, where as trajectories that pass through the thickness of the line will strike the Earth off center. Figure 7 shows the 2036, 2037, and 2051 keyholes for Apophis, the largest keyholes near the predicted 2029 CA trajectory.

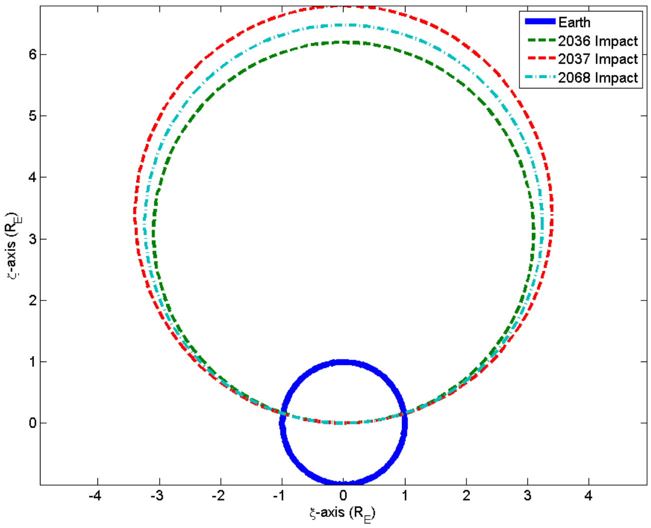

Fig. 7 Valsecchi circles for 2029 CA

Opïk's theory is valid for short encounters, such that the encounter can be approximated by a point. Valsecchi shows that for small values of b, the errors associated with this assumption go to zero with b. On the other hand, as the Tisserand parameter approaches 3, errors associated with this assumption grow. For Apophis, T = 2.967 and U=0.1817. In accordance with the above statements, Opïk's theory and associated analytical geometries provide approximations for keyholes; a dynamic propagator provides more accurate solutions. The fidelity of the solutions generated by Giorgini and Chesley provide this accuracy.

Close approach complexes

Each close approach has a subset of conditions that yield a future impact, i.e. keyholes. In the immediate vicinity of those keyholes exist all the near misses or close approaches for that impact event. Each of those close approaches has a subset of keyholes, and so on. Not all close approaches necessarily have the potential for impact, but these close approaches still affect the orbit. All these close approaches, potentially hazardous or not, form complexes with future close approaches and impacts. Therefore, to fully predict future impacts, a close approach tree must be generated. Fig. 8 shows such a tree (non-comprehensive) for Apophis. The dates in this tree are drawn from (Chesley, 2009).

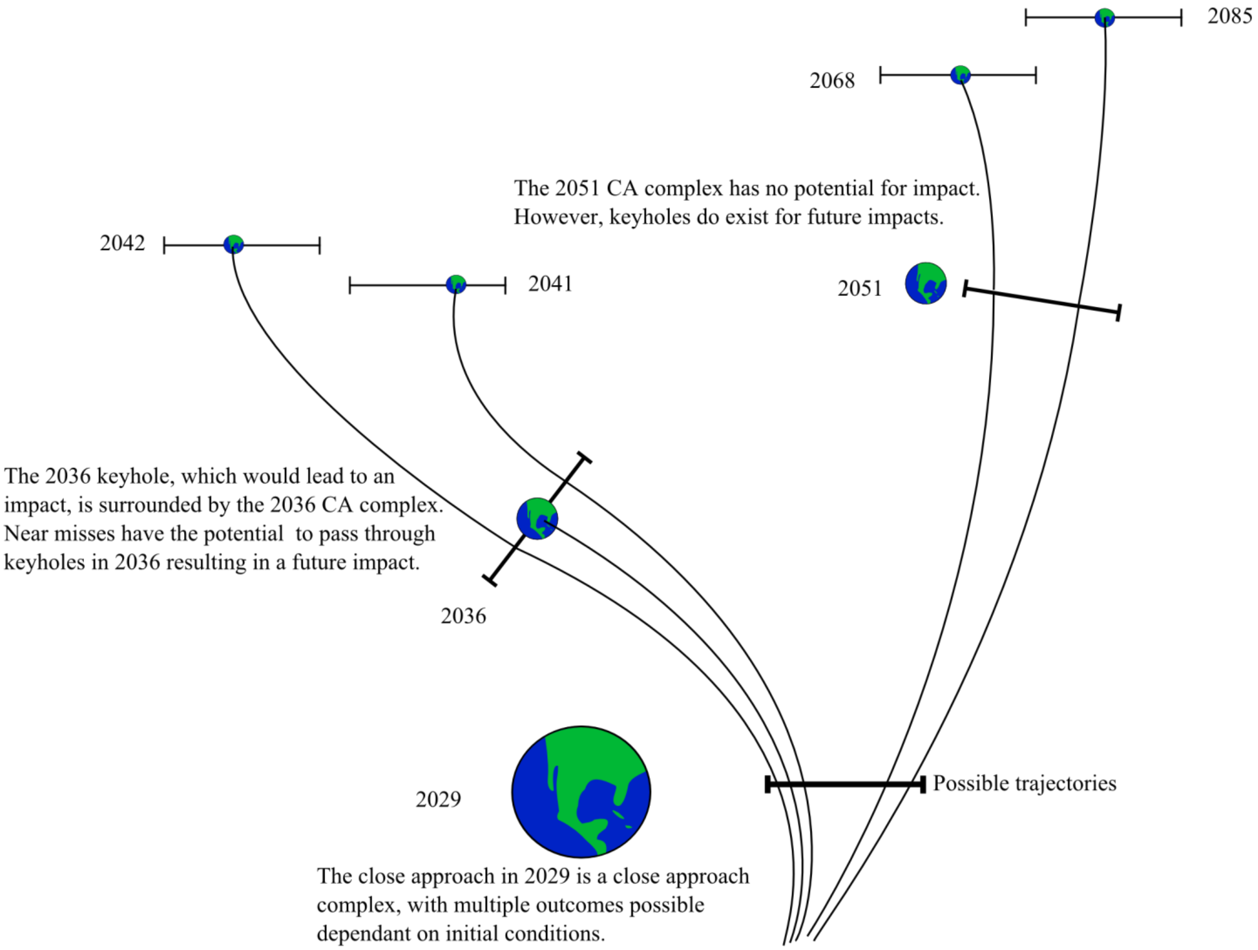

Fig. 8 Close approach branching

III. TRAJECTORY PREDICTION AND UNCERTAINTY

Trajectory prediction, based upon initial conditions and non-linear models, is only as accurate as the preliminary orbit determination and accuracy of the dynamic model. Therefore, the accuracy of the prediction depends on the length of the measurement arc, precision and accuracy of the astrometric observations, and the ability of the model to capture all facets of the non-linear dynamics. Errors accumulate mostly along the track of the trajectory due to four (a, e, ω, t_p) out of six orbital elements contributing to errors in the true anomaly. Error in the true anomaly contributes directly to the timing of the asteroid, whereas small errors have little effect on placement of the impact node. These effects combine to change the predictability of an impact, not the long-term probability of impact. Uncertainty in the solution increases with time and the 2029 CA amplifies those uncertainties.

Giorgini thoroughly analyzes sources of uncertainty in solutions produced by using JPL's SDM. For Giorgini's solution, the standard model is used for orbit determination, whereas an augmented model using a variable order, variable step-size, Adam-Krogh integration is used for prediction. Un-modeled dynamics in the SDM bias the initial conditions and permeate to the prediction through the propagation of those biased conditions. Giorgini classifies physical uncertainty into two groups; Group 1 parameters, which include small effects comparable to integration error and effects unlikely to be measured before 2029; and Group 2 parameters, which stand to be measured or improved before 2029. Group 1 parameters include planetary ephemeris uncertainties (the SDM uses DE405), un-modeled asteroid perturbations, Earth-moon gravitational uncertainty, and integration error. Group 2 parameters include solar energy related perturbations and thermal radiation acceleration.

In 2013, during the CA of Apophis with the Earth, improved astrometry measurements are expected to decrease the positional uncertainty to the order of tens of meters (Giorgini, 2008); some predict estimation of the thermal radiation acceleration and spin-axis from the 2013 observation period using radar-imaging (Chesley, 2009).

Line of variations

While the region of uncertainty for Apophis' position is a three-dimensional ellipsoid, (Chesley, 2009) simplifies this region into a single-dimensioned line of variations as projected on the b-plane. As mentioned earlier, the ς-axis marks the timing coordinate, and, as Chesley shows, the uncertainty in ς is orders of magnitude greater than uncertainty in ξ. Therefore, the uncertainty ellipsoid is projected onto the b-plane as a line of variations (LOV). Figure 9 shows the 2029 LOV in relation to the previously calculated Valsecchi circles.

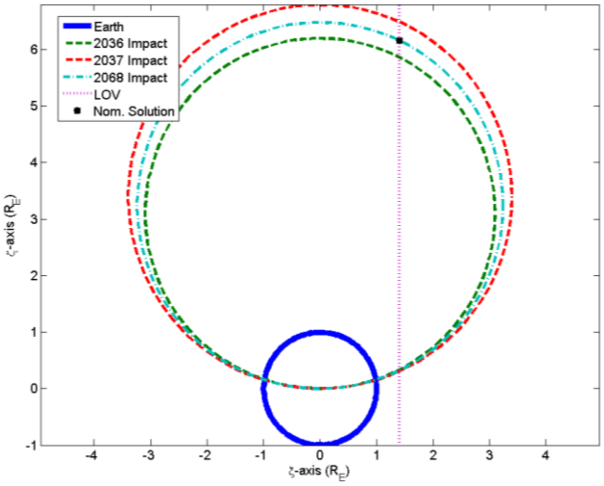

Fig. 9 Line of variations on b-plane for 2029 CA

Keyhole locations within 2100

Chesley (2009) reports the latest solution for Apophis' trajectory based upon updated astrometric measurements (Tholen, 2009), (Giorgini, 2008), and star-catalog de-biasing. Fig. 10 shows the latest solution, 43, with associated 1σ uncertainty and the nearest significant keyholes. As Fig. 10 shows, the nominal solutions lie near the 2 meter wide, 2068 keyhole, and much further from the 600m wide 2036 and 2037 keyholes.

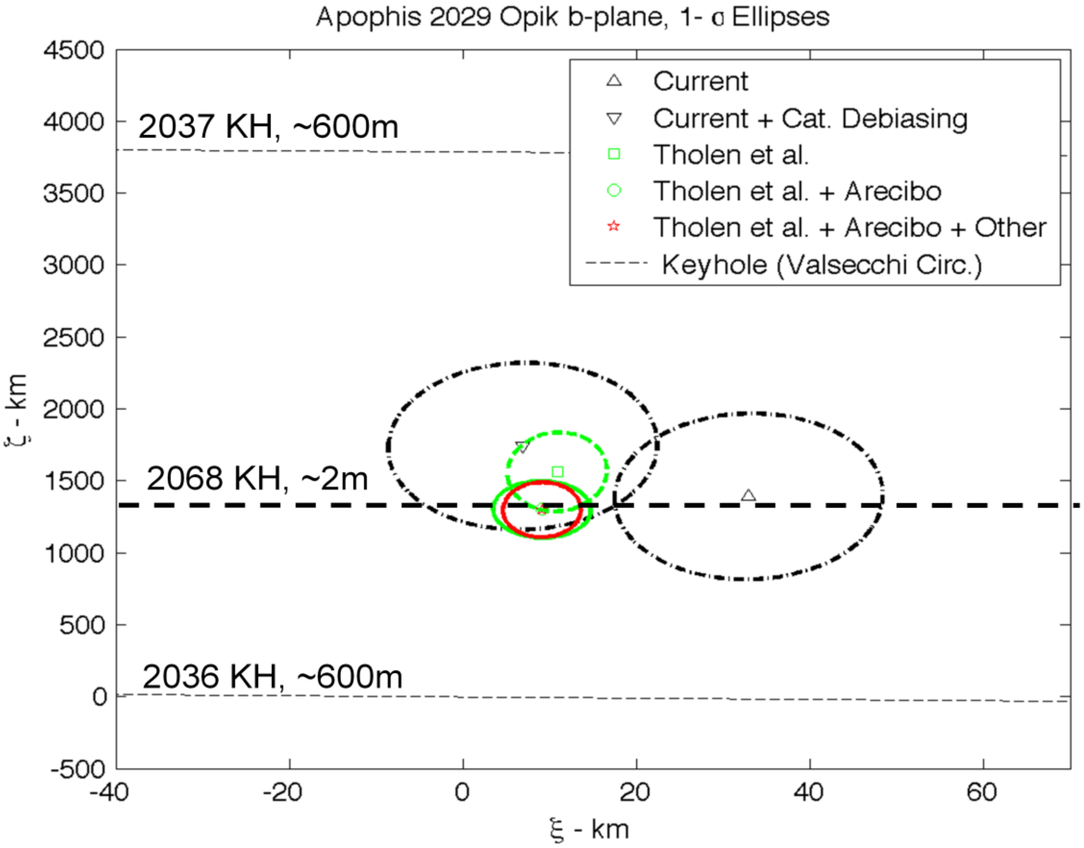

Fig. 10 Solution 43 on 2029 b-plane (Chesley, 2009)

Chesley goes further by projecting all possible solutions along the line of variations until 2100. By tracking the closest approach of each solution, he finds additional keyholes and makes evident the existence of keyhole furcation at close-approach complexes. These complexes represent a miniaturized close-approach event with its own Valsecchi circles and keyholes. As is evident in Fig. 11, many close-approach complexes exist, however two complexes, 2036 and 2051, are more important than others. The former complex is over 100km wide, with multiple potential impacts culminating with the 610m wide 2036 keyhole. The 2051 complex contains a 2m wide keyhole for a 2068 impact.

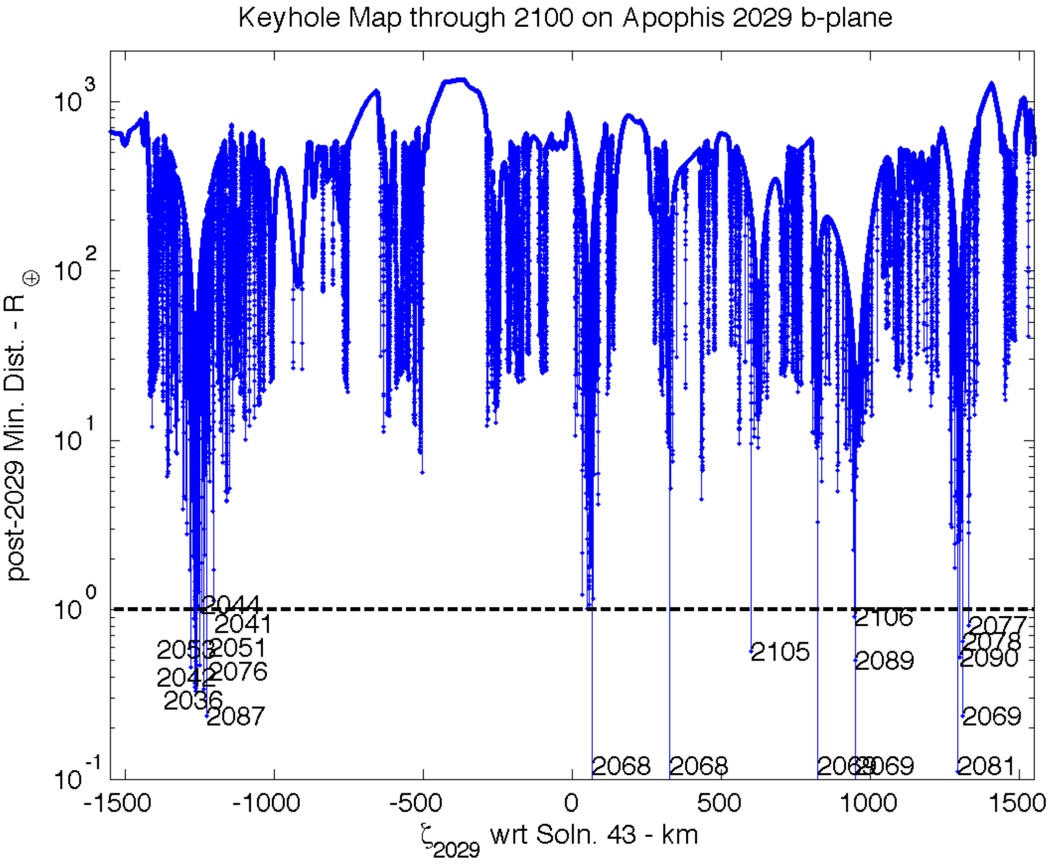

Fig. 11 Keyhole locations within 2100 (Chesley, 2009)

Table 3 shows the most statistically probable keyholes and their parameters. These results are relative to solution 43 (Chesley, 2009), and represent solutions propagated using JPL's SDM.

Table 3
Keyhole locations and associated impacts within 2100 (Chesley, 2009)

Year	Keyhole location from nominal solution (km)	LOV σ	Keyhole width (m)	Impact probability
2036	-1301.7	-3.28	610.	4.5×10^{-6}
2056	17.379	+0.30	0.10	0.1×10^{-6}
2068	28.846	+0.33	2.37	2.5×10^{-6}
2068	288.48	+1.04	0.18	0.1×10^{-6}
2076	34.297	+0.35	0.22	0.2×10^{-6}

These propagations ignore non-gravitational perturbations (NGPs) resulting in two disclaimers on the keyhole position. NGPs affect mainly the timing of the impact (the LOV variable) on the order of hundreds of kilometers per decade. Therefore, the nominal solution is innately flawed in that it does not account for NGPs. Since NGPs require time to make Earth radius sized effects, they do not have much influence on earlier keyholes,. However, later keyholes, and specifically close-approach complexes are altered significantly.

Post 2029 CA nominal and 2051 complex orbits

The 2029 CA will perturb Apophis' orbit substantially. The non-gravitational perturbations on the resulting orbit will vary according the resultant orbital elements. Table 4 shows the post 2029 CA orbital elements. The selection of the CA distances will be discussed in the next section.

Table 4
Post 2029 CA orbital elements

Case	LOV position (from nominal) [km]	a' [AU]	e'
2036 Keyhole	-1300	0.819	0.259
Retrograde	-710	0.822	0.256
In-plane	-20	0.825	0.254
Nominal	0	0.825	0.254
2051 Complex	20	0.826	0.253
Prograde	710	0.835	0.245

IV. NON-GRAVITATIONAL PERTURBATIONS (NGPs)

As mentioned earlier, the JPL SDM does not currently account for non-gravitational perturbations, specifically solar pressure and the Yarkovsky effect (YE). This omission is due to typically, in the cases of km-class or larger objects, insignificance of accelerations caused by these perturbations. However, recent studies of 6489 Golevka (500m diameter) (Chesley, et al, 2003 have shown the YE to produce a measureable effect on Apophis-sized (~270m) asteroids. In the case of Apophis perturbations in the true anomaly and semi-major axis become significant in the time frame of multiple periods. These changes become especially significant due to the magnification of variation in the trajectory caused by the close approach in 2029.

Modeling solar pressure

Solar radiation pressure is caused by the continuous radiation of energy from the sun. This energy interacts with interspatial objects as photons travelling radially from the sun transfer momentum to the objects. Energy absorbed transfers momentum directly, and energy reflected transfers momentum based upon the reflection parameters. Figure 12 shows this event.

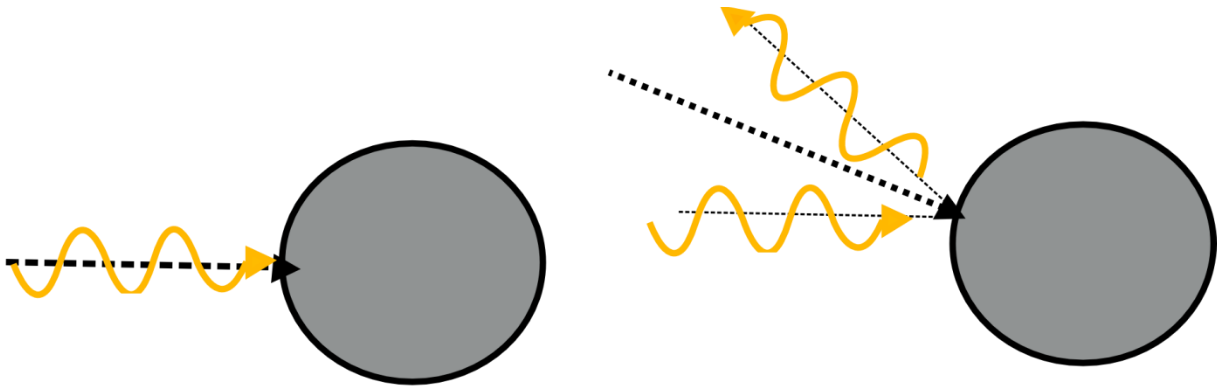

Energy absorbed directly transfers momentum

Reflected energy transfers additional momentum based upon the reflection parameters

Fig. 12 Solar pressure

The solar radiation factor on an spherical asteroid is given as

$$\phi(r) = \frac{\pi R^2 F(r)}{mc} \tag{17}$$

where R is the asteroid diameter; m is the asteroid mass; c is the speed of light; and F(r) is the local flux from solar radiation (Burns, 1979). The local radiation flux can be related to the Earth's mean radiation flux, F_E=1390 W/m^2 (SMAD) by

$$F(r) = \frac{F_E}{r^2} \tag{18}$$

where r is the orbital radius of the asteroid in AU.

The force due to solar pressure is related to the solar radiation by summing absorbed light (inelastic momentum transfer) and twice the retro-reflected light (elastic momentum transfer). Therefore, the radial force due to solar pressure is

$$f_r = \phi(r)(1 + 2A) \tag{19}$$

where A is the Bond albedo.

All bodies interacting with solar pressure are subject to Poynting-Robertson drag (Robertson, 1937). For bodies greater than 0.5 μm solar radiation force is greater than this drag; drag becomes insignificant for objects larger than a few μm. Therefore, for this thesis Poynting-Roberston drag is neglected.

Modeling the Yarkovsky effect

Recent papers by Rubincam, Farinella, and Vokrouhlicky have done much to model the Yarkovsky effect. A recoil force due to re-emission of solar radiation over an anisotropic distribution of surface temperatures, YE is highly dependant on parameters typically unknown for even the most studied objects. YE is a time-varying perturbation based upon two frequencies; the diurnal variant based on rotational frequency, and the seasonal variant based on orbital frequencies. Fig. 13 shows the concept of the Yarkovsky Effect.

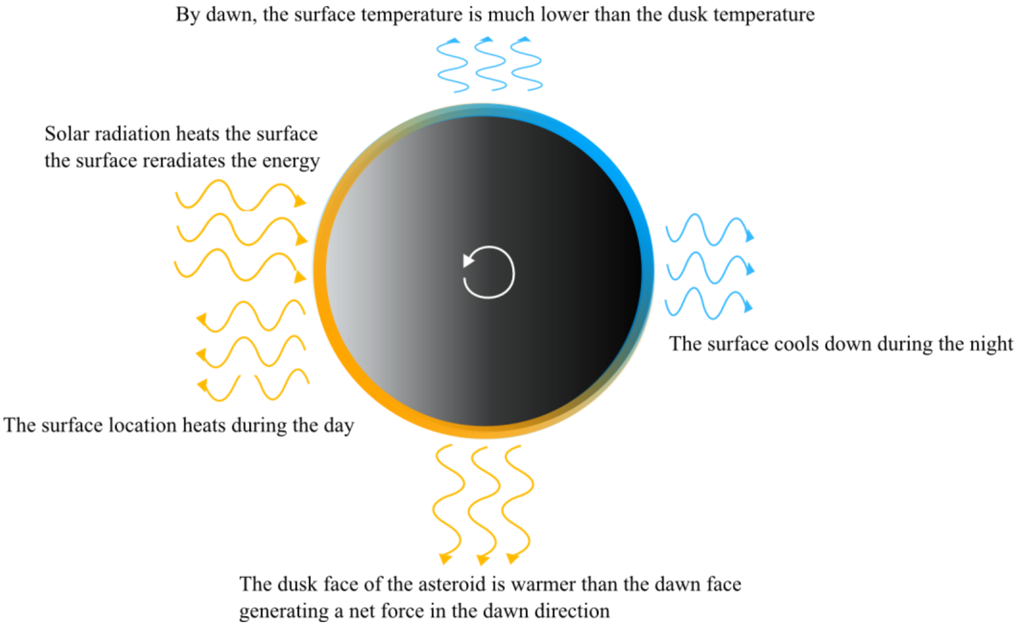

Fig. 13 The Yarkovsky effect

In the linear formulas developed by (Vokrouhlicky, 1998,2000) for the diurnal variant, the orbit is assumed to be circular. This assumption allows for an equilibrium in the asteroid’s mean temperature to be reached; for lightly eccentric orbits this assumption holds as variations in the mean temperature, thermal relaxation, occur over periods much greater than the rotational period. The seasonal variant arises with highly eccentric ($e > 0.3$) orbits and in-plane spin-axes due to the latitudinal fluctuation in absorbed solar radiation. These fluctuations occur over the orbital period of the asteroid and seasonal variant acceleration is aligned with the spin axis of the body. Accelerations due to the seasonal variant are minimal at obliquities nearly prograde or retrograde, and maximum for in-plane axes.

The second basic assumption in (Vokrouhlicky 1998,2000) is that the body is spherical. This assumption is necessary to analyze this problem, but as observations have shown [(Ostro, 1996, 1999) with 1620 Geographos and 4179 Toutatis, and (Abe, 2006) for 25143 Itokawa] this assumption is innately flawed for NEOs. However, this assumption is adopted as a workable approximation in this investigation. Other parameters unknown for Apophis; spin axis, surface thermal properties, and mass; increase the potential error in this modeling, but also alias systematic inaccuracy in the model. Once improved observations or estimations of these parameters become available, a more tailored thermal model may be developed for Apophis.

The local mean temperature T(r) of the asteroid is given as

$$T^4(r) = \frac{\alpha}{\varepsilon\sigma} F(r) \qquad (20)$$

where α is the absorptivity, ε is the emissivity, F(r) the local solar radiation flux, and σ the Stefan-Boltzmann constant.

The mean temperature defines the diurnal thermal parameter, Ξ, as

$$\Xi = \frac{\sqrt{K\rho_s C\omega}}{\varepsilon\sigma T^3(r)} \qquad (21)$$

where K is the thermal conductivity of the surface material, ρ_s is the surface density, C is the specific heat of the surface material, and ω is the rotational frequency of the asteroid. The penetration depth of the diurnal thermal wave, l_d, is

$$l_d = \sqrt{\frac{K}{\rho_s C\omega}} \qquad (22)$$

Vokrouhlicky (1998) shows that the Yarkovsky acceleration is given by

$$f_X + if_Y = -\frac{4\alpha}{9}\phi(r)\frac{\sin\gamma}{1+\lambda}E(R')e^{-i\delta(R')} \tag{23}$$

and

$$f_Z = -\frac{4\alpha}{9}\phi(r)\frac{\cos\gamma}{1+\lambda} \tag{24}$$

where (X,Y,Z) form a coordinate system with Z-axis aligned with the asteroid’s spin-axis, and the X-axis orthogonal to the Z-axis and coplanar with the Z-axis and the orbit radial vector. γ is the obliquity of the spin-axis in relation to orbit radial vector; ϕ is the standard radiation factor described in the previous section. Figure 14 describes the coordinate system.

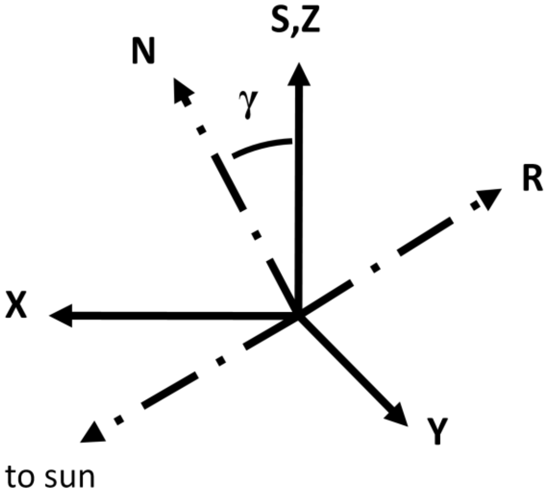

Fig. 14 Yarkovsky coordinate system

The amplitude and phase of $E(R')e^{-i\delta(R')}$ (i is the complex unit) is given as

$$E(R')e^{-i\delta(R')} = \frac{A(R')+iB(R')}{C(R')+iD(R')} \tag{25}$$

where

$$A(x) = -(x+2) - e^{x}[(x-2)\cos x - x\sin x] \tag{26}$$

$$B(x) = -x - e^{x}[x\cos x + (x-2)\sin x] \tag{27}$$

$$C(x) = A(x) + \frac{\lambda}{1+\lambda}\{3(x+2) + e^{x}[3(x-2)\cos x + x(x-3)\sin x]\} \tag{28}$$

$$D(x) = B(x) + \frac{\lambda}{1+\lambda}\{x(x+3) - e^{x}[x(x-3)\cos x - 3(x-2)\sin x]\} \tag{29}$$

and the parameter λ is given as

$$\lambda = \frac{\Xi}{R'} \tag{30}$$

with

$$R' = \frac{\sqrt{2}R}{l_d} \tag{31}$$

Due to the importance of the local dusk direction, a pivotal relationship between spin axis orientation and YE perturbations exists. Prograde rotating asteroids, with dusk facing opposite of the orbital velocity, produce a net force in the orbital velocity direction. Retrograde asteroids produce a net force opposing the orbital velocity. In-plane rotating asteroids produce highly seasonal varying forces. Figure 15 demonstrates the effect of spin axis orientation on YE.

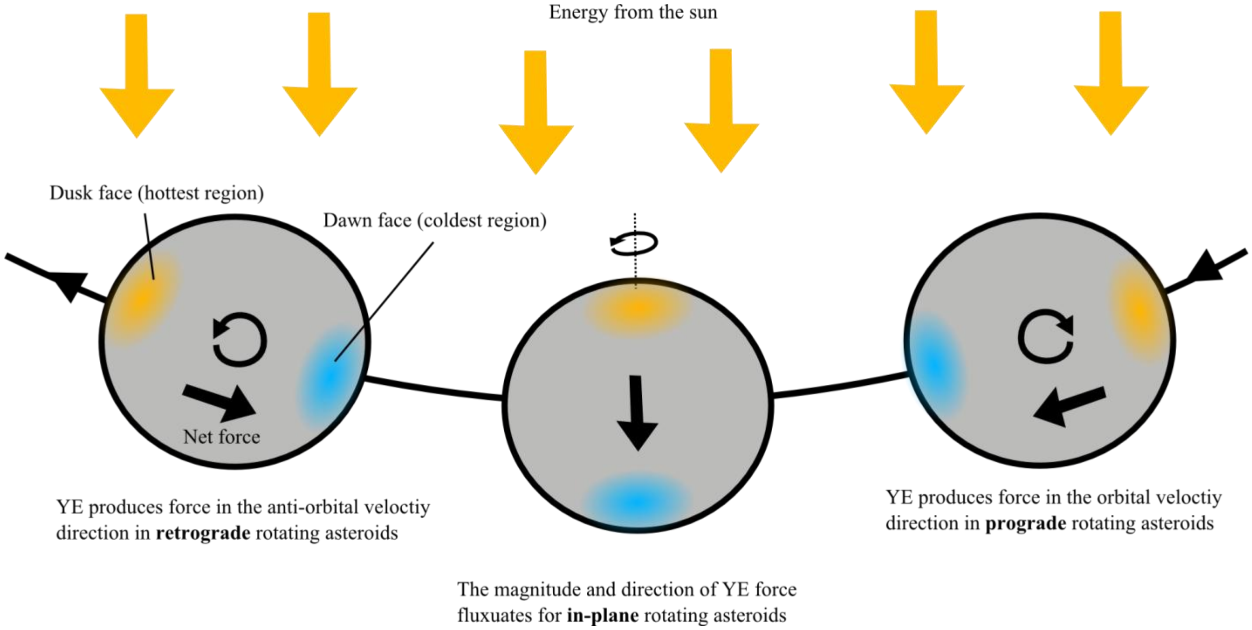

Fig. 15 Spin axis' effect on YE

A "low precision" model of the seasonal variant is analytically derived by (Farinella, 1999). This model is accurate for eccentricities up to 0.4-0.5 (Vokrohlicky, 2000), and will be used because Apophis has a lightly eccentric orbit (e = 0.191). This model is similar to the diurnal variant with acceleration, f_z, which is always along the spin axis. The seasonal variant may be super positioned with the diurnal variant. f_z is given as

$$f_z = \frac{2\alpha}{9}\frac{\phi(r)}{1+\lambda\prime}\sum \chi_k E_k e^{i\delta_k} e^{iMk} \tag{32}$$

where M is the mean anomaly and

$$\lambda' = \lambda(1 - e^2)^{3/8} \tag{33}$$

where in this case, e is eccentricity. The summation is to be performed over all non-zero integers of k, but for low eccentricity orbits the author restricts $|k| < 8$. This restriction is justified because the χ_k factors decay with increasing index k.

$$\chi_k = s_P\alpha_k - is_Q\beta_k \tag{34}$$

where s_P and s_Q are the projection of the spin axis onto the orbit pericenter vector **P** and the vector **Q** being defined as $N \times P$, where N is the orbit normal. The eccentricity dependant functions α_k and β_k are defined as

$$\alpha_k = 2\frac{d}{de}[J_k(ke)] \tag{35}$$

$$\beta_k = 2\frac{\sqrt{1-e^2}}{e}J_k(ke) \tag{36}$$

where $J_k(x)$ are the ordinary Bessel function of the first order and can be found in Battin (1999). The amplitude and phase of E_k and $e^{-i\delta k}$ (i is the complex unit) is given as

$$E_k e^{-i\delta_k} = \frac{A(X_k)+iB(X_k)}{C(X_k)+iD(X_k)} \tag{37}$$

where

$$X_k = \frac{\sqrt{2k}R}{\sqrt{K/\rho Cn}} \tag{38}$$

where n is the mean motion.

Apophis' physical properties

When estimating the impact of NGPs on Apophis' trajectory, the asteroid diameter, geometric albedo, Bond albedo, bulk density, total porosity, mass, surface density and conductivity, and spin axis are factors. Current estimates on the values are derived from limited Earth-based measurement and empirical data gathered from similar asteroids. Prior to 2029, future Earth-based observations may produce improved radar imagery for diameter, volume, albedo, and spin axis orientation; measurements of Yarkovsky based accelerations also allow calculation of mass and bulk density (Chesley, 2003).

Using polarimetry gathered during four observation periods, at four different phase angles, (Delbo et al, 2007) derive an albedo of 0.33±0.08. Delbo assumes, using for the IAU H-G two-parameter magnitude system, the G slope parameter to be 0.25, which is common for S and Q class asteroids (Bowell, 1989); the absolute magnitude, H, calculated is 19.7±0.3. Using the measured albedo and absolute magnitude, Delbo calculates the diameter of Apophis at 270±60m. The equation

$$D = \frac{1329}{\sqrt{p_v} \times 10^{H/5}} \tag{39}$$

relates geometric albedo and absolute magnitude to diameter. Fig. 16 shows this relation as it will be utilized for this thesis.

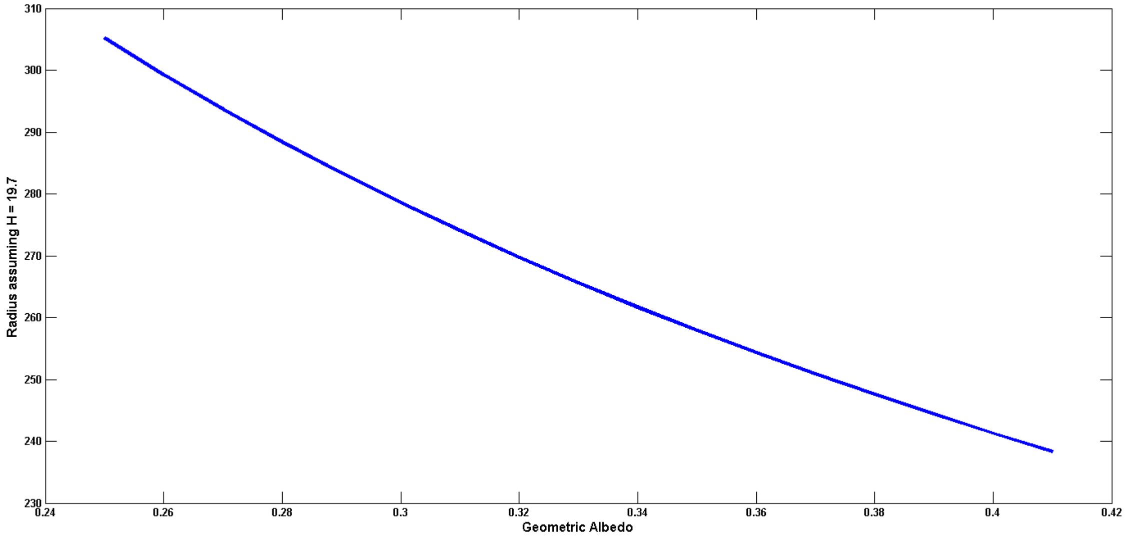

Fig. 16 Relation between diameter and geometric albedo

Apophis is determined to be a Sq-class asteroid composed of mainly olivine and pyroxene (Binzel et al, 2009). This classification indicates a strong similarity to the spectral properties of LL-chondrite meteorites; physical characteristics of these bodies have been studied in the laboratory environment. Using these characteristics and a total porosity of 0.72, the mass is estimated at $2.4\text{x}10^{10}$kg. Similarly, measurements taken by the Hayabusa spacecraft of the asteroid 25143 Itokawa (Abe et al, 2006), show a total porosity of 0.60; if Apophis is assumed to have the same porosity as Itokawa, the mass of Apophis would then be $2.0\text{x}10^{10}$kg.

(Bottke et al, 2006) places the surface density and thermal conductivity at 1.7g/m^3 and 0.01 $Wm^{-1}K^{-1}$ respectively. The difference compared with the bulk density is due to the porous regolith that gathers on the surface. The surface conductivity is dependant upon the surface porosity; values can be as low as 0.001 $Wm^{-1}K^{-1}$ for highly porous regolith, 1.0 $Wm^{-1}K^{-1}$ for ordinary chondritic bare-rock, or as high as 40 $Wm^{-1}K^{-1}$ for iron-rich meteorites.

The Bond albedo, A, is related to the geometric albedo, p_v, through the phase integral, q. $A = p_v \times q$. The phase integral can be calculated as $q = 0.290 + 0.684 \times G$, where G, the slope parameter, is assumed to be 0.25. This yields a phase integral of 0.46, which when combined with geometric albedo of 0.33, produces a nominal Bond albedo of 0.152. Absorptivity is the fraction of energy absorbed by the surface material. This value can be taken as unity less the Bond albedo. (Müller, 1999) reports the emissivity of chondritic asteroids at 0.9 using photometric observations. (Ghosh, 1999) reports the most commonly accepted value for the specific heat of chondrites is 1200 J/kg/K.

Presently, little is known about the spin axis of Apophis. Light curves obtained by (Behrend, 2004) clearly show a rotational period of 30.6 hrs, but give little insight to Apophis' spin-axis orientation. As we have seen, uncertainty in the spin-axis orientation has a major effect on the magnitude and direction of NGPs; we will consider in-plane, prograde, and retrograde orientations as limiting cases. (La Spina, 2004) reports that of 21 NEAs studied, 14 were retrograde, with 9 having spin axes of less than -45° obliquity. This retrograde excess allows the author to produce probabilities, but no additional assumptions are made regarding spin axis orientation.

This thesis looks at the effects of non-gravitational perturbations on possible cases that exist for Apophis' physical properties and initial conditions to yield understanding on possible mitigation strategies. Table 5 shows the nominal values and ranges of physical properties that will be used for the remainder of this thesis.

Table 5
Apophis' physical properties

Property	Nominal	Min Value	Max Value	Source
Diameter (m)	270	210	330	Delbo, et al, 2007
Absolute magnitude	19.7	20.0	19.4	Delbo, et al, 2007
Geometric albedo	0.33	0.25	0.41	Delbo, et al, 2007
Bond albedo	0.152	0.115	0.189	-
Absorptivity	0.85	0.81	0.89	-
Emmisivity	0.9			Müller, 1999
Bulk density (g/cm^3)	3.2	3.0	3.4	Binzel, et al, 2009
Total porosity	0.60	0.38	0.96	Binzel, et al, 2009
Mass (x10^{10}kg)	2.0	0.7	6.1	Binzel, et al, 2009
Surface density(g/cm^3)	1.7			Bottke, 2006
Surface conductivity (W/m/K)	0.01	0.001	0.1	Bottke, 2006
Rotational frequency (Hz)	9.08E-6			Behrend, 2004
Specific heat (J/kg/K)	1200			Ghosh, 1999

Effect on the nominal trajectory

Due to uncertainty in the asteroid parameters, mainly mass/albedo, and the spin axis, nine cases are investigated to demonstrate the effect non-gravitational perturbations have on the nominal trajectory of Apophis. Three spin states; prograde, retrograde, and in-plane; and the albedo/mass states; nominal values, least reflective, most massive; most reflective, least massive; are selected to demonstrate the variations. Table 6 summarizes the nine aforementioned cases.

Table 6
Limiting cases on asteroid parameters

Case	Spin axis	Bond Albedo	Radius	Mass [x10^{10}kg]
Prograde/Nominal	Prograde	0.152	270	2.0
Retrograde/Nominal	Retrograde	0.152	270	2.0
In-plane/Nominal	In-plane	0.152	270	2.0
Prograde/Most Massive	Prograde	0.115	330	6.1
Retrograde/Most Massive	Retrograde	0.115	330	6.1
In-plane/Most Massive	In-plane	0.115	330	6.1
Prograde/Least Massive	Prograde	0.189	210	0.7
Retrograde/Least Massive	Retrograde	0.189	210	0.7
In-plane/Least Massive	In-plane	0.189	210	0.7

The author simulates non-gravitational perturbations using Cowell's method, using a Runge-Kutta routine to integrate at each variable time step. The coding is written in Matlab, and the results presented are product of those simulations. Fig. 17 shows the variations in the orbital elements from the date of the nominal solution obtained from JPL ephemeris data, January 2010, through April 2029 due to solar pressure and YE. Both cyclical variations with orbital frequency, and secular growth is shown.

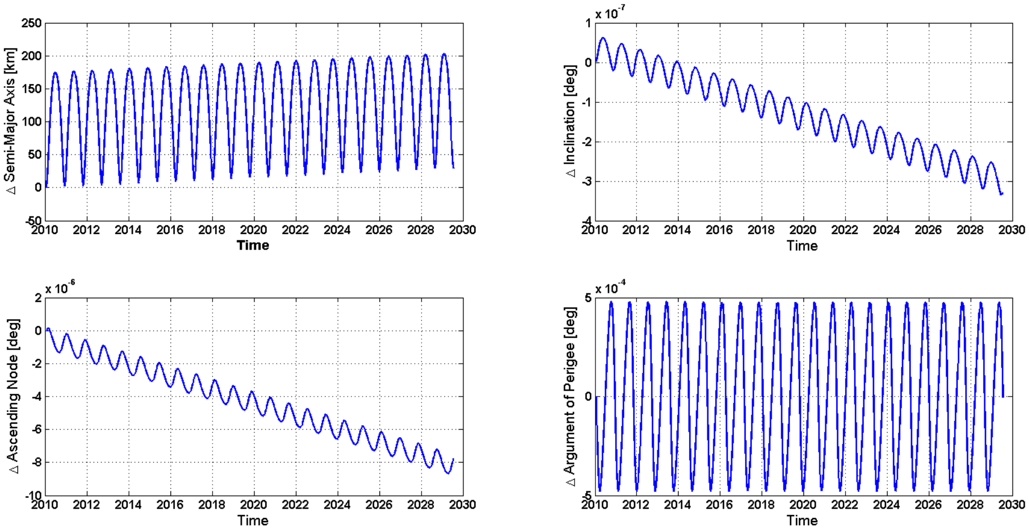

Fig. 17 Variations in the orbital elements (nominal mass, prograde spin)

As shown in Fig. 17, variations in semi-major axis are proportional to time, $\Delta a \propto t$. Alternately, variations in true anomaly, *f*, are proportional to the square of time, $\Delta f \propto t^2$. As discussed earlier, variations in the ς-axis are more easily obtained due to relation to the true anomaly, *f*. Variations in position on the ς-axis, Δx, are proportional to variations in true anomaly. (Vokrouhlicky, 2000) demonstrates this relation, and the author adapts the units of that equation to yield

$$\Delta x \approx 10.5 \frac{\left({n_P}/{10} \right)^2}{{a_{AU}}^{3/2}} \dot{a_P} \qquad (40)$$

which approximates Δx in km, where n_p is the number of periods from initial time to final time, the initial semi-major axis is in AU, and $\dot{a_P}$ is the secular change in semi-major axis per period.

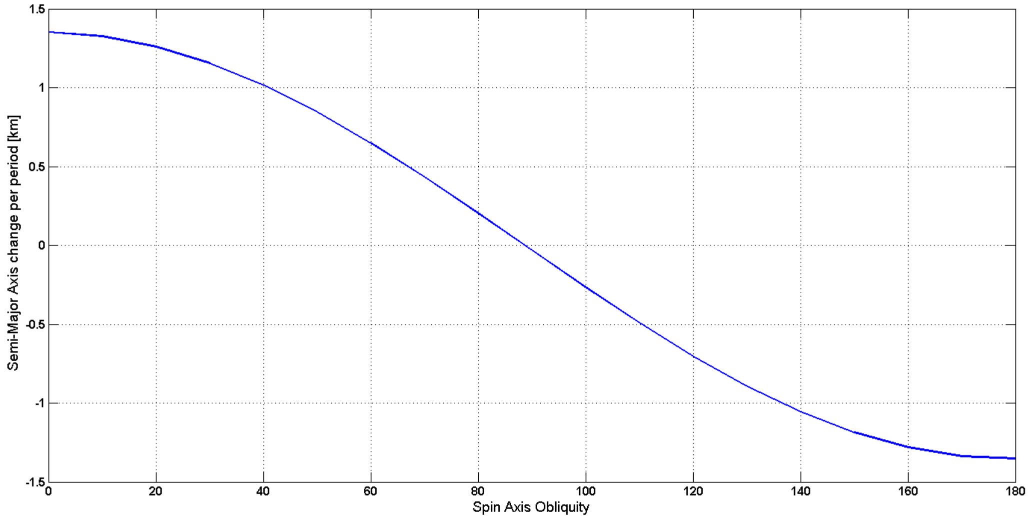

Fig. 18 da/dP vs. spin axis obliquity (nominal mass)

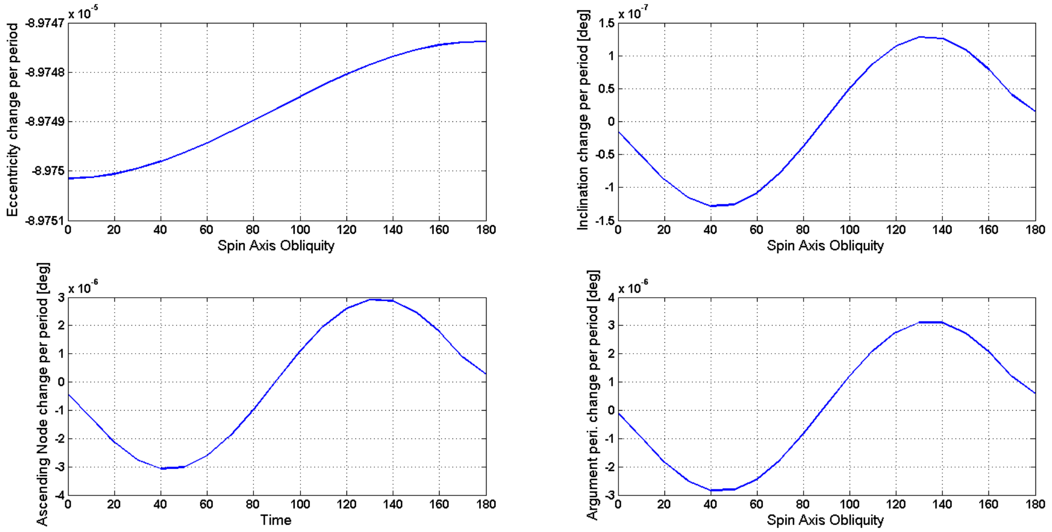

Fig. 19 Variations in the orbital elements per period vs. spin axis obliquity (nominal mass)

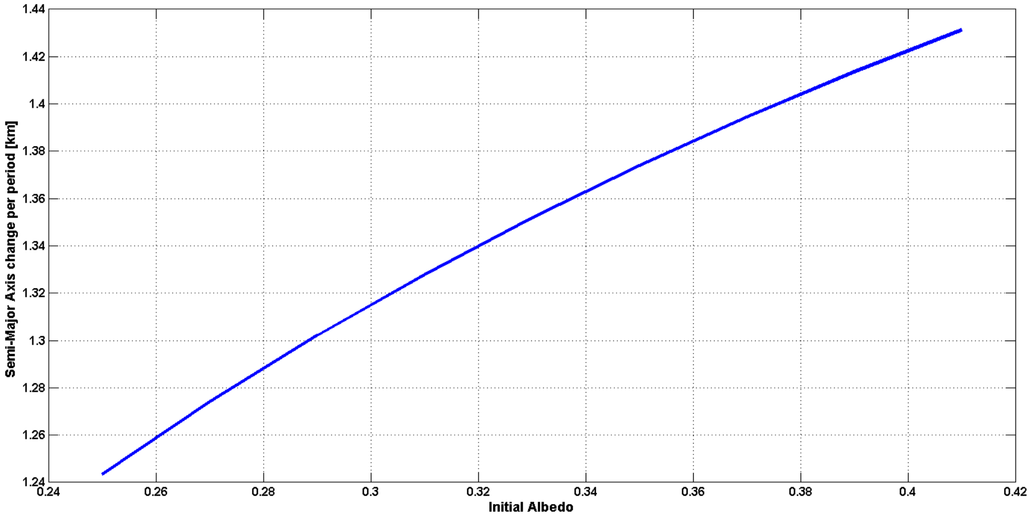

Fig. 20 da/dP vs. initial albedo (prograde spin)

Fig. 18 and Fig. 19 show the relation of variations in the semi-major axis to variations in the spin axis obliquity and other orbital elements for nominal mass and reflectance of the asteroid. Similarly, Fig. 20 shows the relation to initial albedo and therefore mass of the asteroid. The variation in semi-major axis behaves as predicted, growing with prograde spin axis and decreasing with retrograde spin axis. The less reflective, more massive cases vary less due to non-gravitational perturbations and more reflective, less massive cases vary more. Additional plots regarding orbital element variations are shown in Appendix C.

Table 7 summarizes the orbital element variations for each of the nine-cases listed in Table 6. The final column in Table 7 shows the final variation in x at the 2029 CA.

Table 7
Orbital element variations per period

Case	d*a*/dP [km]	d*i*/dP [x10^{-8}°]	dΩ/dP [x10^{-7}°]	dω/dP [x10^{-7}°]	Δx LOV [km]
Prograde/Nominal	1.35	-1.5	-4.6	-1.2	706
Retrograde/Nominal	-1.35	1.5	2.4	5.8	-706
In-plane/Nominal	-0.0327	0.62	0.38	1.7	-17.1
Prograde/Most Massive	1.24	-1.4	-4.2	-1.2	649
Retrograde/Most Massive	-1.24	1.4	2.1	5.1	-649
In-plane/Most Massive	-0.0300	0.56	0.24	1.5	-15.7
Prograde/Least Massive	1.43	-1.6	-4.8	-1.2	748
Retrograde/Least Massive	-1.43	1.6	2.6	6.3	-748
In-plane/Least Massive	-0.0345	0.67	0.48	1.8	-18.0

Following a probabilistic approach, three cases are run to demonstrate the uncertainty in 2029 position due to variations in the albedo. Fig. 21 shows 3000 normally distributed cases for initial albedo, and Fig. 22 shows the variation in semi-major axis under three spin cases for the varying albedo. Finally, the keyhole positions are adjusted nominal trajectory for the 2029 CA in km. This adjustment is shown in Appendix D. Due to uncertainty in the albedo, keyholes in close proximity to each other encounter aliasing.

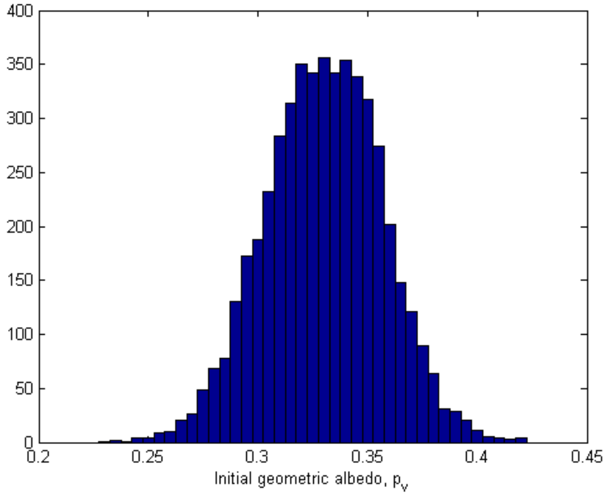

Fig. 21 Albedo variation for 3000 normally distributed cases

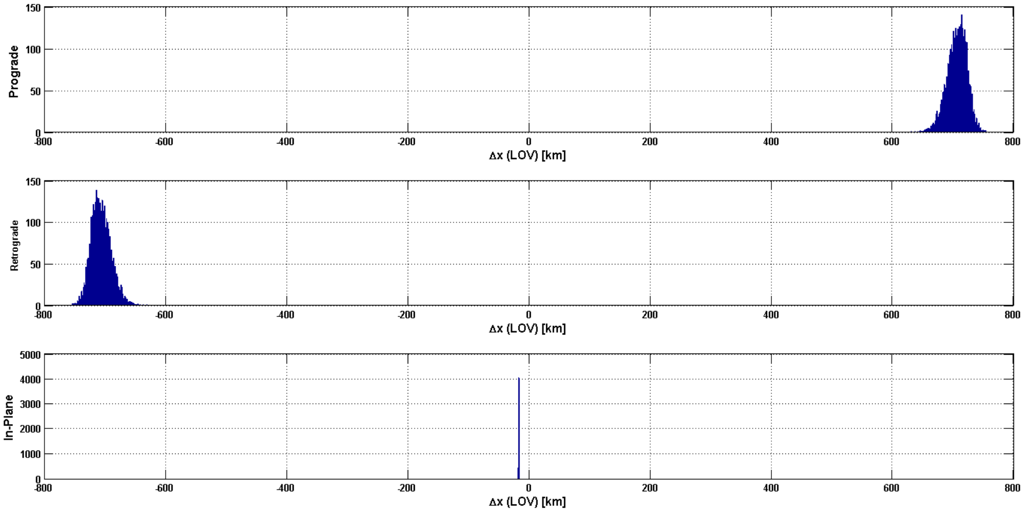

Fig. 22 Probability of variations in da/dP due to uncertainty in albedo

The total probability for the LOV variation due to NGPs is presented in Fig. 23. The property uncertainties are listed in Table 8. This result gives the additional uncertainty provided by NGPs to the uncertainty in LOV position in 2029. Fig. 24 shows the distribution of physical properties over 10000 cases.

Table 8
Total property uncertainty in 2010

Property	**Nominal value**	**3σ uncertainty**
Spin axis*	-π	±7/12π
Geometric albedo	0.33	±0.01
Surface density [kg/m3]	1700	±200
Specific heat [J/kg/K]	1200	±200
Thermal conductivity [W/m/K]	10^{-2}	[10^{-1}, 10^{-3}]

* Retrograde excess in spin axis is approximated by the normally distributed random function $= -\pi \pm \frac{7}{12}\pi$.

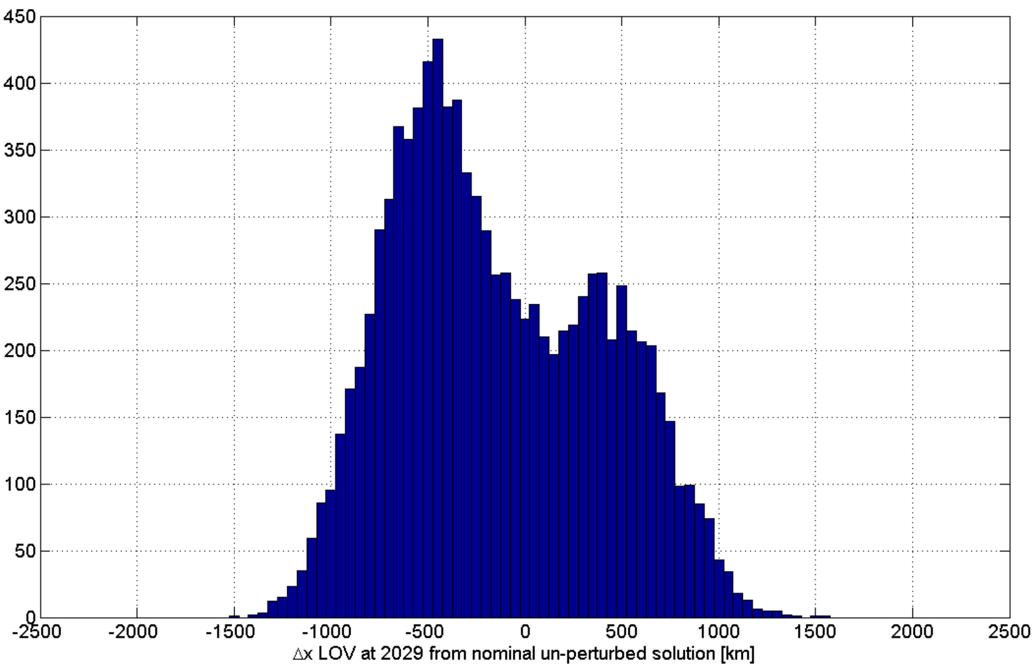

Fig. 23 Total probability of Δx at 2029 CA

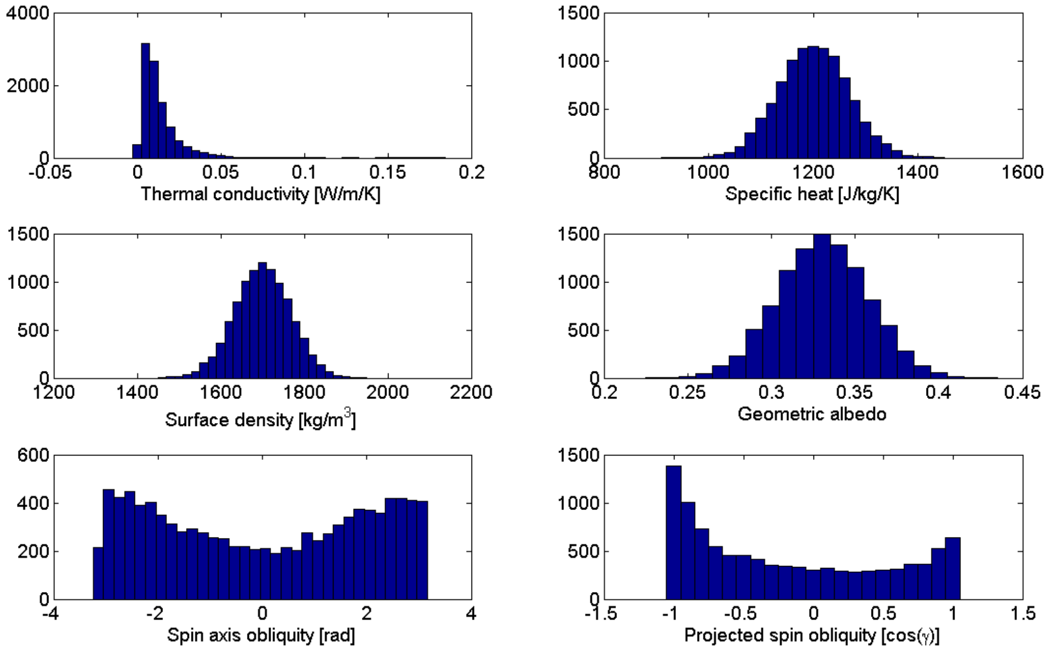

Fig. 24 Distribution of physical properties at 2010

Fig. 23 shows that uncertainties in Apophis' 2029 position due to NGPs are significant and of the order of orbit determination uncertainty. There are two definite peaks at ±500km resulting from the two dominant spin orientations. The retrograde excess increases the probability of the -500km peak.

The results obtained in this section are consistent with results from (Giorgini, 2008) and (Chesley, 2009). Giorgini reports NGPs shifting Apophis trajectory by 320-750km between 2006 and 2029 for non-in-plane cases, and 10-20km for in-plane cases. Chesley reports a similar plot to Fig. 23 with peaks at ±300km.

Post 2029 CA non-gravitational perturbations

To investigate the most probable outcome of the 2029 CA, the non-gravitational perturbations are calculated for a series of orbits that may result. The first set is related to the nominal orbit solution accounting for NGPs, these cases are shown continuing the assumes spin state. The second set is related to keyholes; the 2051 CA being possible with a range of spin states, and the 2036 keyhole being only probable with a retrograde spin state. The results are shown in Table 9.

Table 9
Post 2029 CA non-gravitational perturbations

Case	Spin	LOV position (from nominal)	da/dP [km]	Δx [km]
2036 Keyhole	Retrograde	-1300	-0.94	-8.5
Retrograde	Retrograde	-710	-0.95	-
In-plane	In-plane	-20	-0.023	-
2051 CA	Prograde	20	0.96	-84
	In-plane		-0.023	2.0
	Retrograde		-0.96	84
Prograde	Prograde	710	1.0	-

NGPs have negligible effect on the 2036 impact post 2029 CA, 9km << 1R_E. However, keyholes in the 2051 CA are significantly effected by NGPs post 2029 CA. If the keyholes in 2051 are assumed to be on the same order of magnitude of the 2029 CA keyholes, an 84km shift in the nominal path for Apophis between 2029 and 2051 will change the location of the keyholes in the 2051 CA substantially.

The impact node will evolve due to non-gravitational perturbations. The result of each close approach will yield varying orbital elements. But if the order of magnitude for the non-gravitational perturbations is preserved (for non-in-plane cases), the MOID will exceed the Earth's sphere of influence (~1x10^6km) within 1My. This estimate is consistent with Morbidelli's NEO lifetime figure.

V. MODIFYING ALBEDO

As shown in the previous sections, variations in solar pressure and thermal radiation acceleration, both dependant on geometric albedo, have major effects on the location of the 2029 CA and beyond. This section details a technique for modifying the albedo developed by the Texas A&M University Apophis Study Group (TASG). The technique utilizes the natural charging of regolithic bodies and industrial powder coating technology in the form of tribo-electrification.

(Pellazari, 1978), (Whipple, 1981), and (Lee, 1996) discuss the natural charging of objects in space. First noticed during the Apollo missions, electrostatically charged particles are present on all regolithic bodies that interact with the sun. The surface regolith becomes charged by being stripped of electrons by the solar wind. Whipple reports that the sunlit prominences on the lunar surface may have an electric charge between 0 and +20V, where as the dark side may be as negative as -1800V. Furthermore, electrostatically levitated particles exist in a cloud above positively charged surfaces. Evidence of these effects were seen by Apollo crews when they interacted with negatively charged particles as they passed as high as 100km above the surface. Horizon glow at lunar sunsets also provide evidence of this effect. Lee calculates a sunlit surface charge for an asteroid at 3 AU to be 5V. Assuming a relation $V \propto 1/r^2$ and re-evaluating for an asteroid between 1 and 0.75 AU yields a surface charge as high as 45-80V, respectively. Figure 25 shows the static charging of asteroids due to solar radiation.

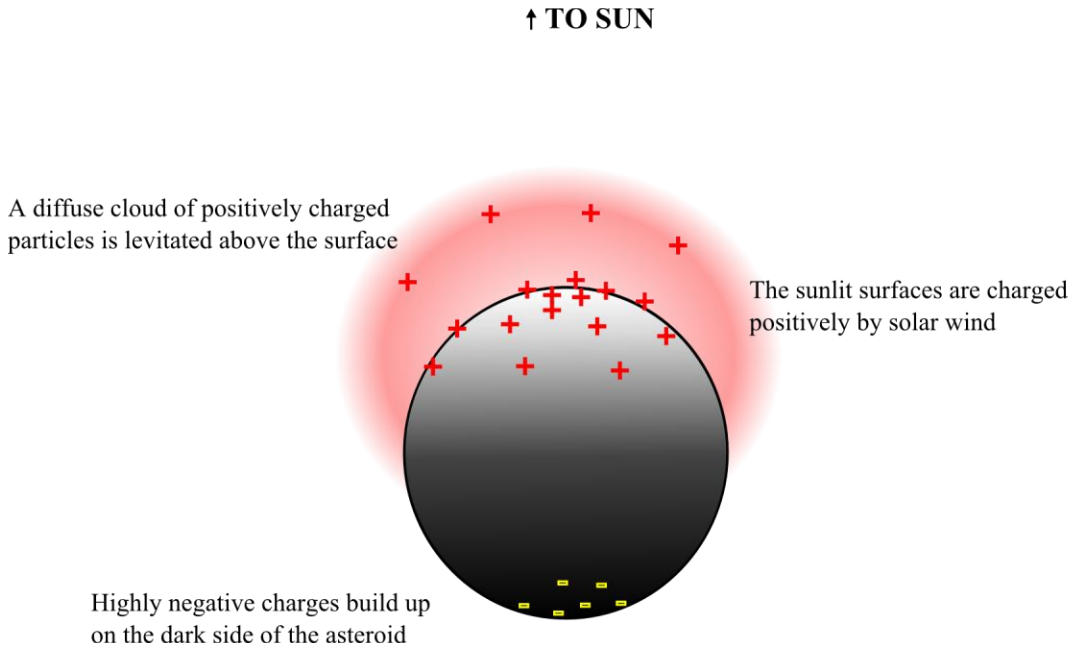

Fig. 25 Static charging of asteroids due to solar radiation

Application of ACPs

The NEO mitigation technique first presented by (Hyland et al, 2009a) takes advantage of natural charging on sunlit surfaces of NEOs. By charging a fine powder material, the electrostatic attraction between the albedo change particles (ACPs) and the surface augments the miniscule (~$1\text{x}10^{-4}$ m/s^2 at the surface) gravitational attraction of Apophis. The ACPs are charged using the developed technology of tribo-charging. In triboguns, the particles are charged through collisions with the barrel (Masuda, 1976). The powder and barrel material must be selected to be both distant on the tribo electrification series and have the acceptor's work function be much greater than the donor's. Table 10 shows a list of possible materials for both barrel and powder. Since the asteroid surface is positively charged, the ACPs must be negatively charged. In terrestrial applications, the particles are propelled through the mechanism using compressed air; a space-based system, the Albedo Change Mechanism (ACM) will use compressed inert gas, such as nitrogen for the same function.

Table 10
Material Selection [Engineering Toolbox]

Material	**Electron Donor or Acceptor**	**Polymer Type**	**Density (kg/m^3)**	**Thermal conductivity [W/m/K]**	**Specific Heat**
Nylon	Donor	Thermoplastic	1130	-	-
Polyvinylchloride (PVC)	Acceptor	Thermoset	1340	0.19	1050
Polytetrafluoroethylene (PTFE)	Acceptor	Thermoset	2200	0.25	1170
Polypropylene	Acceptor	Thermoplastic	900	0.15	1000

Once propelled from the spacecraft, the ACPs will be attracted to the surface via gravitational and electrostatic attraction. From a distance, the net charge of the asteroid will attract the particles, but as the ACPs approach the surface, variations in surface charge will influence the particles. This influence is beneficial because shadowed regions, which affect albedo less than sunlit regions, accumulate negative charge, repelling the particles to positively charged regions on the surface. As the particles strike the surface, they will discharge and will adhere to the surface material. The ACPs will be sized to avoid levitation; the material will be selected to melt under direct sunlight at 1 AU intensities. By melting the particles, the powder will cure into a thinner sheet that covers more surface area. Additionally the curing will crosslink material from different particles and form bonds with the surface material. Figure 26 shows how ACPs are deposited on the surface.

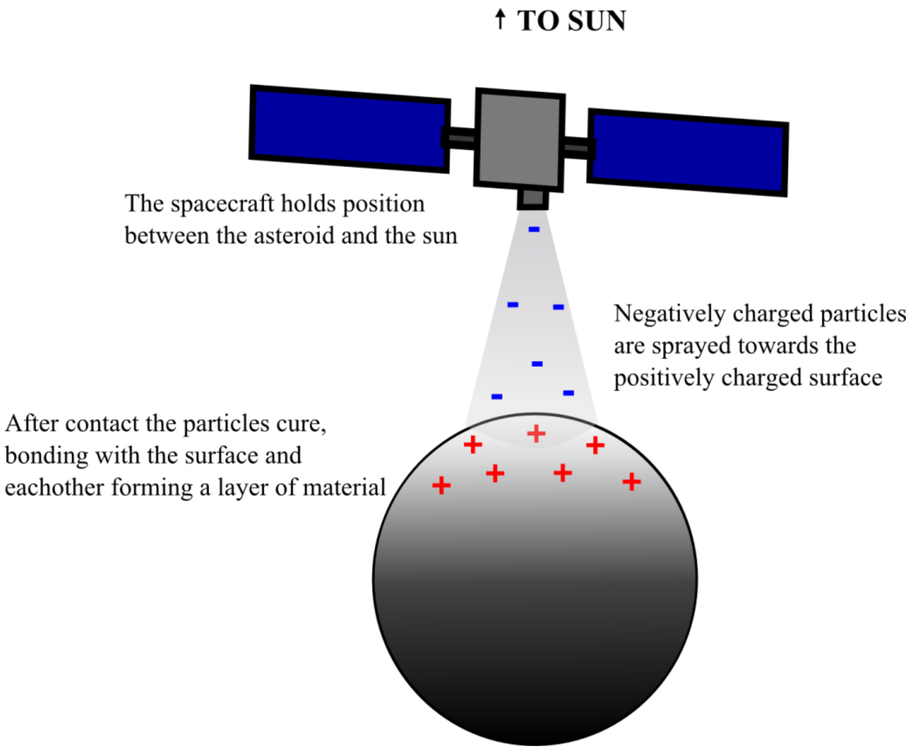

Fig. 26 Deposition of ACPs on surface using tribo-charging

Powders have distinct advantages over the method of albedo change suggested by (Giorgini, 2008), a thin fabric solar sail deployed on the surface. Powders can be applied between 30-50μm in thickness requiring more mass than 5-10μm sheet of carbon nano-tubes. However, this mass is more than accounted for in the simplicity of deployment compared with the solar sail. Whereas the deployment of powders requires a tribogun mechanism and associated powder storage and plumbing with a mass on the order of 10-20% of the material, solar sail deployment would require a complex method to deploy the sail flatly and securely on the surface of the asteroid. This mechanism could be multiple times more massive than the material.

The goal of the tribo gun shall be to generate as much negative charge per particle as to ensure attraction to the surface, where the solar energy activated curing process will adhere the particle to the surface and generate a thin coating. Masuda reports the charge per mass, q/m_p or electric current per powder mass flow rate, $I_m/\dot{m}$, as

$$\frac{q}{m_p} = \frac{I_m}{\dot{m}} = \frac{\varepsilon_0 |V_c| \Delta x \Delta t S}{m_p z_0 \tau} \frac{\Delta n}{\Delta x} \tag{41}$$

where ε_0 is the dielectric constant of the propellant medium; V_c is the contact potential difference; Δx is the pipe length; Δt is the contact duration; $\Delta n/\Delta x$ is the number of collisions per unit length; S is the contact area; z_0 is the gap between contact bodies; and τ is the relaxation time of the particle, given as the product of the internal resistance and capacitance.

Modeling modification

By applying a cured layer of ACP's to the surface of Apophis, the covered area's properties are being altered. In terms of initial albedo, p_{vi}, and ACP surface albedo, p_{vp}, the final albedo, p_{vf}, can be calculated by

$$p_{vf} = \frac{(4\pi R^2 - A'_p) p_{vi} + A'_p p_{vp}}{4\pi R^2} \tag{42}$$

where R is the asteroid radius, and A'_p is the spherically projected area of the modified surface.

The spherically projected area of the modified surface differs from the actually area covered by ACP material due to porosity of the rock and associated shadowing effects. Fig. 27 shows that on Itokawa approximately 5% of the surface area is shadowed to some extent. Additional, unseen surface exists as well on side and bottom faces of boulders. These surfaces do not contribute to the spherically projected area that constitutes the albedo, but may be covered with ACP material. Therefore shadow efficiency, η_s, relates the spherically project area to the total area covered by ACP material, A_p as

$$A'_p = A_p \eta_s \tag{43}$$

Depositing ACPs on the sunlit face of the asteroid serves to maximize efficiency, but complete efficiency is not expected. Experimentation and simulation needs to be completed to better estimate this value, but for the purposes of this thesis, a shadow efficiency of 0.9 is assumed.

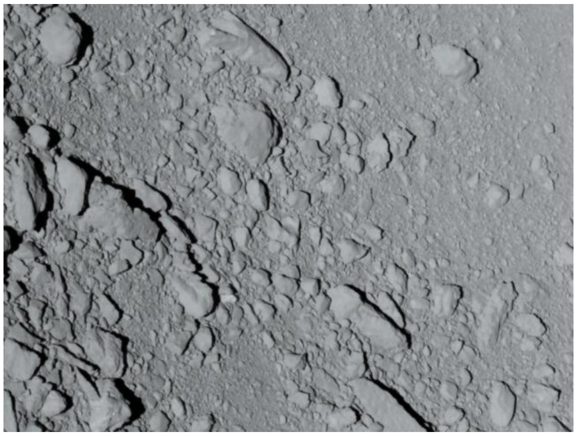

Fig. 27 Shadowing on Itokawa [JAXA]

The mass of ACPs required to produce the desired final albedo calculated as

$$M_p = \rho_p \tau_p A_p \tag{44}$$

where ρ_p is the density of the ACP material, and τ_p is the average thickness of the ACP coating. A_p can be solved for in term of the initial asteroid parameters and the desired albedo as

$$A_p = \frac{4\pi R^2 (p_{vf} - p_{vi})}{\eta_s (p_{vp} - p_{vi})} \tag{45}$$

Maximum modifications under limiting cases

Utilizing the formulae developed above, the mass required for limiting cases is computed for each material in Table 11; both increasing and decreasing the average geometric albedo by 0.005 are calculated. The calculation assumes the relation between diameter and initial albedo described by Delbo and an average coating thickness of 30 µm. Powders increasing the asteroid albedo have an albedo, $p_{vp} = 0.85$, where as powders decreasing are $p_{vp} = 0.05$. These assumed values are compatible with modern satellite paints (SMAD).

Table 11
Mass required to modify albedo

Material	**Max mass to increase 0.005 (kg)**	**Nominal mass to increase 0.005 (kg)**	**Max mass to decrease 0.005 (kg)**	**Nominal mass to decrease 0.005 (kg)**
PVC	110	100	340	190
PTFE	180	160	530	290
Polyproylene	70	60	210	110

Fig. 28 and Fig. 29 demonstrate the relation between required powder mass and initial albedo of the asteroid. Because the diameter of the asteroid decreases with increasing initial albedo, the decreasing mass required with increasing initial albedo is caused by the decreasing area to be modified. The disparity between masses required to increase and decrease the final albedo is due to the difference in p_{vp} and p_{vi}. Nominally, the Δp_v or change in albedo per unit area for the light powder is 0.52; for the dark powder, $\Delta p_v = -0.28$. Correspondingly, the area to be modified for the dark powder is larger than for the light powder.

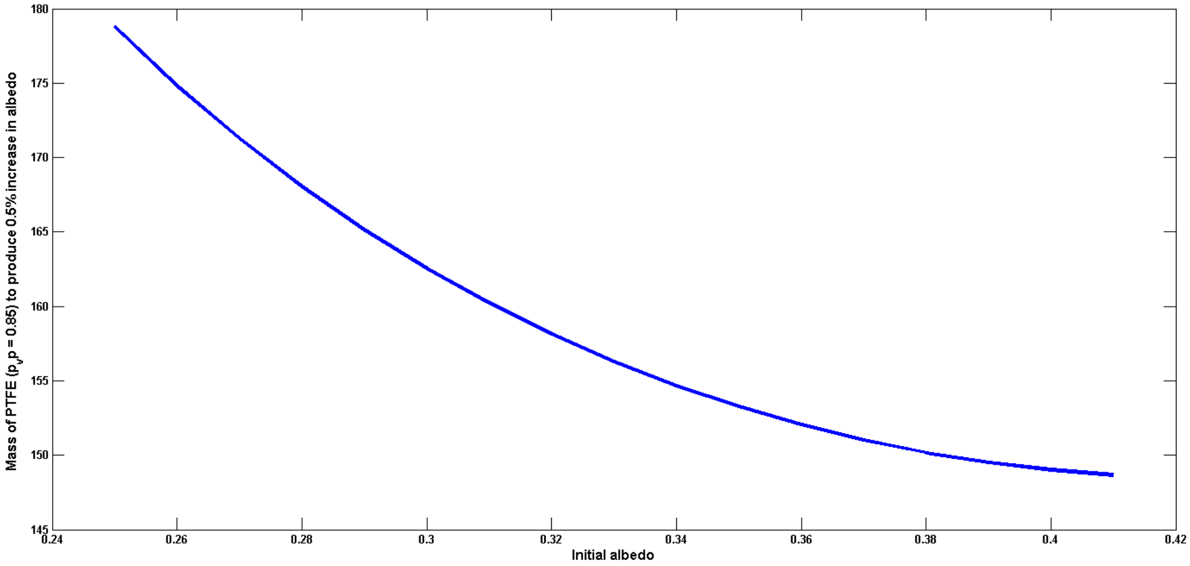

Fig. 28 Mass of PTFE required to increase average albedo by 0.5%

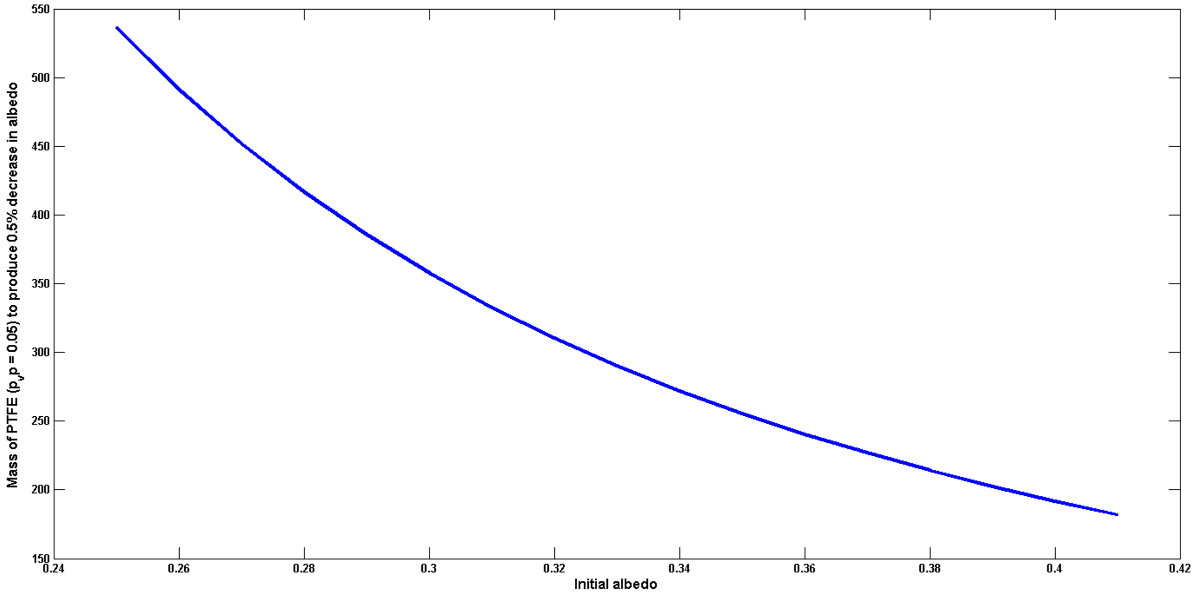

Fig. 29 Mass of PTFE required to decrease average albedo by 0.5%

The surface properties will be modified by the coating of powder. These properties are not limited to absorptivity and emissivity. As the thermal wave penetration is on the order of

0.01m, and the powder thickness is on the order of 10^{-4}m; modification to the thermal penetration depth, l_{df} is also incurred,

$$l_{df} = \sqrt{\frac{K_f}{\rho_{sf} C_f \omega}} \tag{46}$$

where the formula for modified K_f, ρ_{sf}, and C_f are given by

$$\Gamma_f = \frac{\left(4\pi R^2 l_d - A'_p \tau_p\right)\Gamma_i + A'_p \Gamma_p \tau_p}{4\pi R^2 l_d} \tag{47}$$

with Γ being the surface property. l_d must be solved for using Newton's method. Fig. 30 shows the change in thermal penetration depth due to application of PTFE as related to the change in albedo desired. By increasing the thermal penetration depth, the effective radius, R', is reduced, retarding the YE.

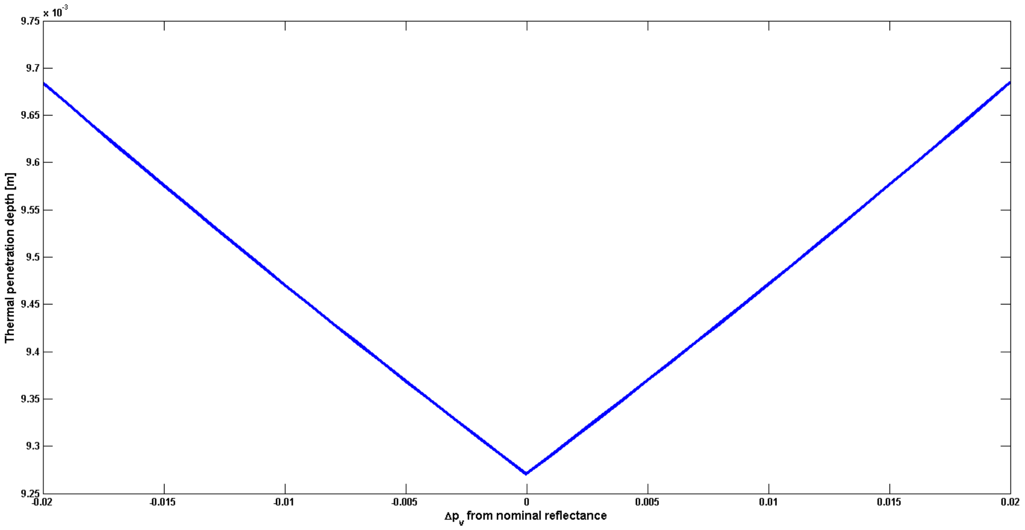

Fig. 30 Thermal penetration depth vs. desired change in albedo

The AEMP mission

(Hyland, et al, 2009b) incorporate this technique into the Apophis Exploration and Mitigation Platform, a mission to study and track Apophis such that possible impacts can be mitigated using gravity tractoring and the aforementioned albedo change technique. From “A Mission Template for Exploration and Mitigation of Potentially Hazardous Near Earth Asteroids” (Hyland, et al, 2009b):

> The AEMP spacecraft is designed as a Discovery class mission with a cost under \$350 million. The mission utilizes a Falcon 9 launch vehicle to place the spacecraft in an Earth escape trajectory and a Star 30BP solid rocket motor to provide the rendezvous ΔV. The spacecraft will be operated semi-autonomously with high-level commands and programming uploaded via a high-gain link. A gimbaled, high gain antenna and an omni-directional low gain antenna will be mounted on the spacecraft. The Deep Space Network (DSN) will be employed for communications with Earth. The spacecraft will be 3-axis stabilized with reaction wheels and attitude control motors. A Star Tracker is to be used for attitude determination, with an Inertial Measurement Unit (IMU) and radio positioning for inertial navigation. An Optical Navigation Camera and Laser Range Finder (LRF) will determine relative position to the asteroid. A dual-mode propulsion unit will perform trajectory correction maneuvers and proximity operations. Power will be provided through a common bus, with Lithium-Ion battery packs and fixed deployable solar panels. The spacecraft launch mass is estimated to be 1100kg, with a post-rendezvous mass of 560kg at Apophis.
>
> The baseline mission profile consists of six phases: launch, rendezvous, pre-mitigation exploration, short term mitigation, long term mitigation, and post-mitigation

investigation. During the launch and rendezvous phases, the spacecraft is launched into an intercepting orbit and uses impulsive maneuvers to rendezvous with the asteroid, where the primary mission begins. During the pre-mitigation exploration phase the spacecraft will maneuver about the asteroid, serve as a platform to study the physical properties of the target object, and refine estimates of the trajectory. This information will be transmitted to an Earth-based team to determine the method and parameters of mitigation. After sufficient models have been formulated, the short term mitigation phase begins by positioning the spacecraft at a standoff near the asteroid. Two Hall thrusters are used to maintain the spacecraft position, imparting a small amount of force on the asteroid through mutual gravitation. The mitigation must take place before the 2029 close approach to yield maximum effect in 2036.

Following a period of intermediate analysis to observe the effects of the gravity tractoring, the spacecraft will close within 100m of the surface of Apophis and activate the tribogun. The spacecraft will maintain inertial position utilizing the powder expulsion as propulsion depositing the material across the surface of the asteroid as the asteroid rotates beneath the spacecraft. During the post-mitigation investigation, the spacecraft will verify the effects of the two mitigation techniques. In particular, the albedo modification technique is examined to determine the efficacy of the albedo change method and subsequent effects on the trajectory.

To safely alter Apophis’ trajectory, the initial orbit must be determined and propagated accurately. The AEMP mission will track Apophis originally, reducing uncertainty in the initial conditions; study Giorgini’s group 2 parameters to better calculate the non-gravitational perturbations; and after two years of tracking, better determine the actual effect these perturbations have on Apophis' orbit. Appendix E details the AEMP mission concept. Table 12 shows a science traceability matrix for the AEMP payloads.

Table 12
AEMP science traceability matrix (Hyland, 2009b)

	Optical Navigation Camera	Laser Range Finder	Radio Science	Inertial Measurement Unit	Star Tracker	Micro-Bolometer
Determine Absolute Position of Spacecraft			**x**			
Determine SC to Apophis relative position	**x**	**x**			**x**	
Determine mass of Apophis	**x**	**x**	**x**	**x**		
Map surface geometry	**x**	**x**				
Determine bulk volume and density	**x**	**x**				
Model the gravity field	**x**	**x**				
Map the albedo of the Apophis	**x**	**x**				**x**
Determine average bond albedo	**x**	**x**				**x**
Map surface temperature						**x**
Determine spin axis	**x**					

Tracking accuracy is predicted for a spacecraft using a deep space beacon in conjunction with the Deep Space Network (DSN) [Hyland et al]. The deep space beacon can take four measurements; time of travel ranging, delta differential one-way ranging (ΔDOR), Doppler range-rate, and altitude and azimuth using very-long-baseline interferometry. The measurements, when filtered by an unscented Kalman filter (UKF), provide 100m 3σ precision. Assuming tracking begins in late 2022 and continues until late 2024, as the AEMP concept prescribes, Apophis trajectory can be predicted within 0.0001 Earth radii (2000m) at the 2029 CA. This prediction precludes ground based measurements available during 2013, 2021, and 2029 CA events. However, if the possibility of impact is high enough based upon 2013 observations, a mission to deflect Apophis the less than 300m, in AEMP’s case using a combination of gravity tractoring and albedo modification, required to avoid keyholes in 2029 would need to launch by 2021 to be successful.

VI. AVOIDING EARTH IMPACT USING ALBEDO MODIFICATION

To assess the ability of albedo modification to avoid keyholes, the effect of albedo modification is tested on nominal and limiting cases. The results, similar to (Giorgini, 2008) are shown in Figure 31. The results are the total displacement in 2029 following modification in 2023, as per the AEMP mission concept. Similarly, Fig. 32 shows the total displacement while adjusting for changes in surface properties due to powder deposition.

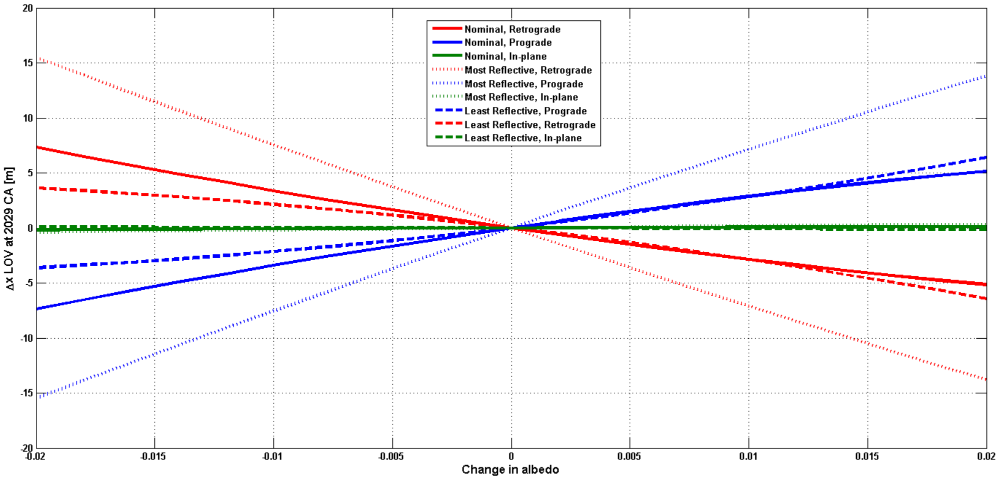

Fig. 31 Δx due to albedo change by 2029

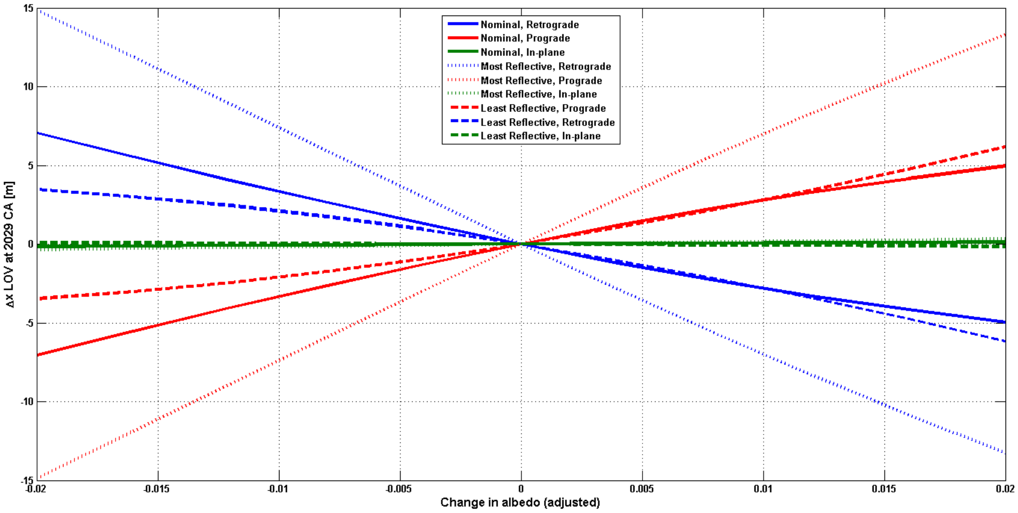

Fig. 32 Δx due to albedo change by 2029 (adjusted)

Spin axis orientation has a major effect on the effectiveness of this method. Modification to in-plane spin axes cases has little effect on the asteroid position at 2029. Conversely, the non-in-plane cases with 2% alterations produce deflections greater than 4m by 2029. The less massive cases are more heavily influenced by the modifications, producing up to 15m deflection in 6 years.

Avoiding keyholes

Next in assessing the ability of albedo modification to avoid keyholes, the remaining uncertainty of the NGPs is investigated. A few assumptions are made about the knowledge of Apophis' state in 2014, the time when development of a mission to Apophis would need to be started. These assumptions are based on the expected observations in 2013. The first is assuming that the spin state is known to 3σ uncertainty to 5°. The second is that the initial albedo is known to 3σ uncertainty within 0.01 of the nominal value of 0.33; the radius being related to this number is also constrained. These assumptions are consistent with previous radar observations of asteroids (Ostro, 1996). The values for surface density, specific heat, and thermal conductivity are shown with these assumptions in Table 13.

Table 13
Assumed property uncertainty at 2014

Property	**Nominal value**	**3σ uncertainty**
Spin axis	[-90°, 0°, 90°]	±5°
Geometric albedo	0.33	±0.01
Surface density [kg/m3]	1700	±200
Specific heat [J/kg/K]	1200	±200
Thermal conductivity [W/m/K]	10^{-2}	[10^{-1}, 10^{-3}]

Fig. 33 and Fig. 34 show the distribution of physical properties and the uncertainty in 2029 position due to NGPs. 5000 cases were run for each of the spin axis cases.

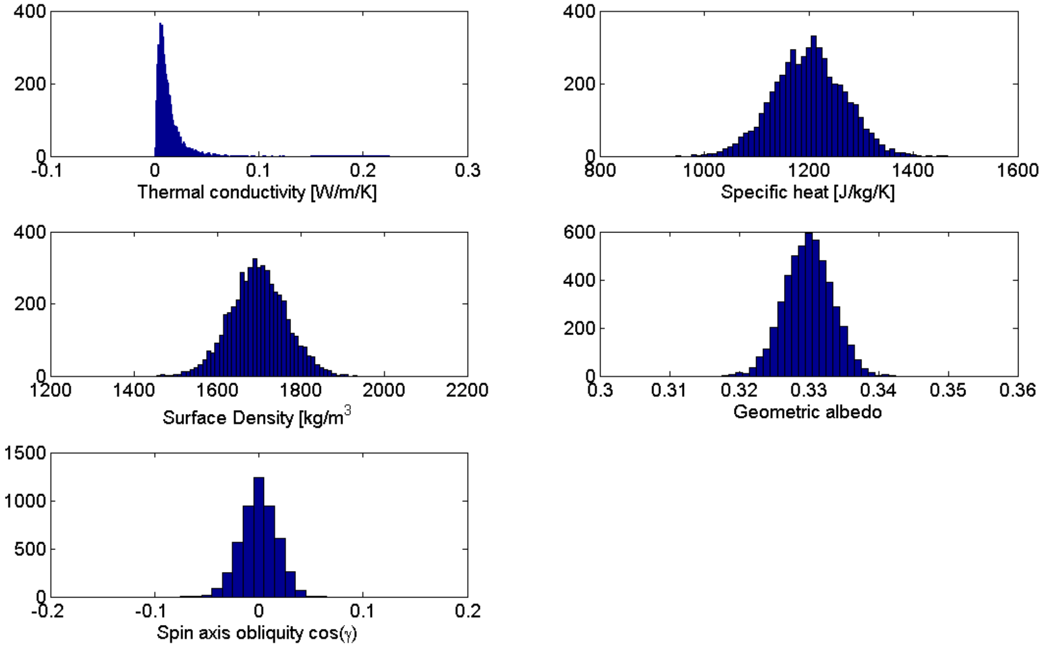

Fig. 33 Assumed property distribution at 2014

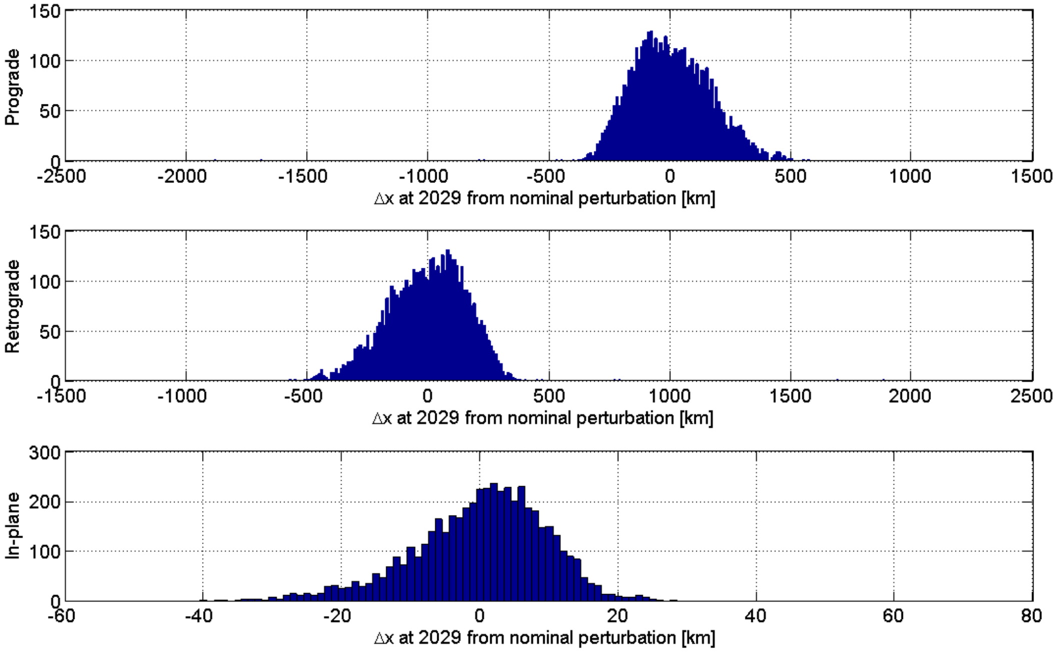

Fig. 34 Assumed keyhole uncertainty due to NGPs at 2014

The uncertainty in 2029 LOV position due to variations in NGPs stems from uncertainty in the physical properties. The uncertainty tends to skew the NGPs toward less effective, i.e. the mode resulting LOV value for prograde spins is less than the nominal case. The standard deviation for the non-in-plane spin cases is 180km offset by ±40km, and 8km offset by 3km for in-plane cases. The most significant cause of uncertainty is the thermal conductivity. Because the thermal conductivity varies by one order of magnitude in either direction, the thermal penetration depth, which is proportional to the magnitude of NGPs, varies by orders of magnitude. Therefore, while radar observations in 2013 predict the general direction of the NGPs, further study on the physical properties, specifically thermal conductivity, is required to predict the magnitude of these effects. However, if the asteroid is observed to have a retrograde spin axis, the nominal and uncertain cases would fall between the 2036 and 2051 CA complexes with no known keyholes that would yield impacts before 2100.

Next, uncertainties due to NGPs are studied on the eve of the mitigation technique being performed. This study assumes that a transponder-beacon spacecraft has tracked Apophis to sub 100m accuracy, study the physical properties of the asteroid, and investigates the remaining uncertainties in 2029 position due to NGPs. Table 14 shows the assumed uncertainty remaining for Apophis’ physical properties. Fig. 35 shows the distribution of these properties for 5000 cases, and Fig. 36 shows the resulting variations in 2029.

Table 14
Assumed property uncertainty at 2023

Property	**Nominal value**	**3σ uncertainty**
Spin axis	[-90°, 0°, 90°]	±1°
Geometric albedo	0.33	±0.001
Surface density [kg/m3]	1700	±50
Specific heat [J/kg/K]	1200	±50
Thermal conductivity [W/m/K]	10^{-2}	[$10^{-1.9}$, $10^{-2.1}$]

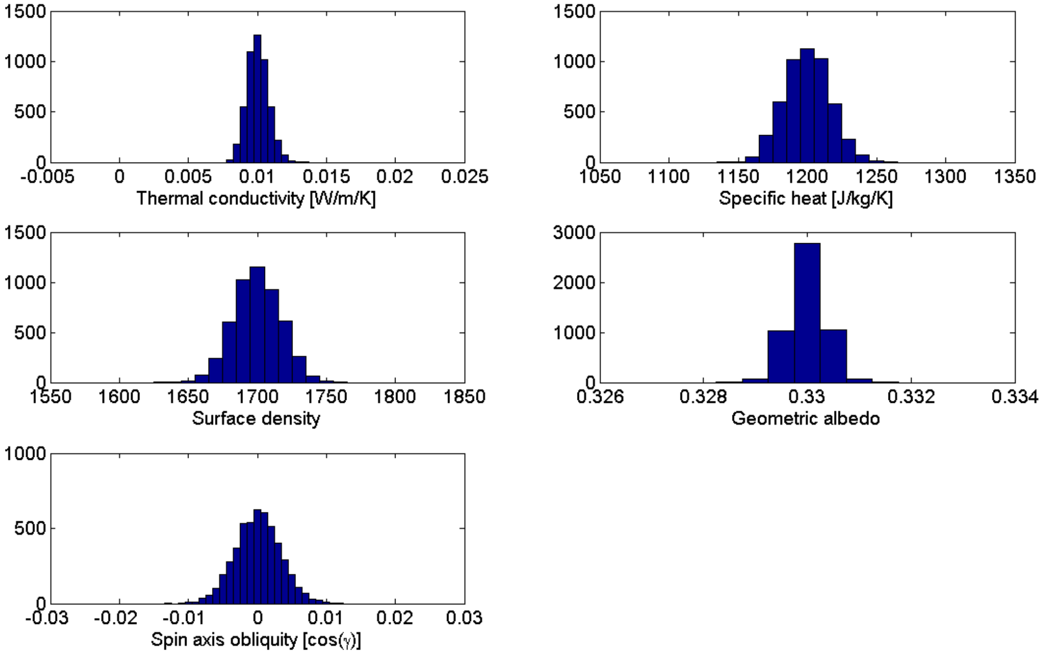

Fig. 35 Assumed property distribution at 2023

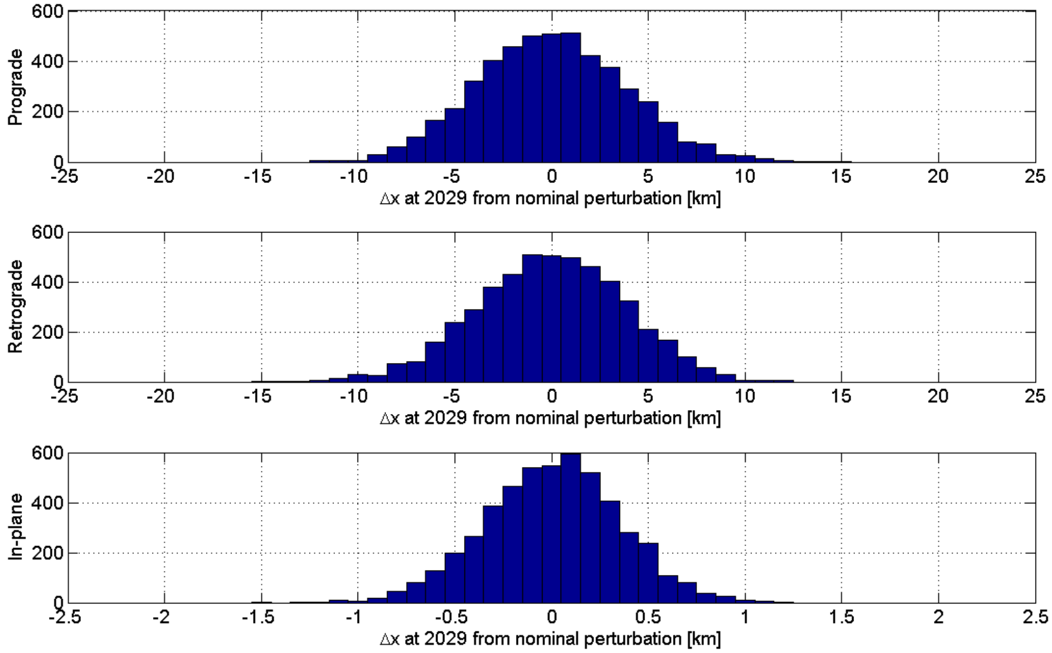

Fig. 36 Assumed keyhole uncertainty due to NGPs at 2023

Due to the decrease in propagation time and the narrowing of uncertainty in physical properties, the uncertainty in Apophis position in 2029 is narrowed. The standard deviation for the Δx results are 4km for the non-in-plane cases, and 0.35km offset by 0.1km for the in-plane cases. Combined with improved orbit determination, these results would be able to definitively eliminate all possibilities for passing through keyholes (if this were the case).

Based on the previous results, the effectiveness of modifying the albedo is only feasible if the prediction of NGPs can be as precise as ~10m. While Fig. 36 shows otherwise, solving for NGPs can be achieved in ways other than observation of physical properties. One such case is studying the direct effect of NGPs on Apophis' orbit over a long observation arc. Secular NGPs could potentially be extracted to yield the required precision. Certainly by 2023, the magnitude of the NGPs could be observed.

VII. CONCLUSION

As this thesis has shown, the NEO 99942 Apophis poses a potential impact threat in the near term and for the foreseeable future. Based upon orbit determination uncertainty and non-gravitational perturbation uncertainty, Apophis has the potential to pass through one of multiple keyholes during the 2029 CA which would lead to an impact in the future.

Non-gravitational perturbations caused by interaction with solar radiation cause secular perturbations on Apophis' orbital elements. These perturbations yield a total displacement of up to ±1500km between 2010 and 2029. These perturbations continue to affect Apophis after the 2029 CA.

A novel technique to modify the albedo of Apophis, and therefore alter the NGPs was investigated. 100kg of albedo changing powder was shown to be able to produce ~10m deflections of Apophis between 2023 and 2029 for non-in-plane spin axes of Apophis. This timeline is consistent with the AEMP mission proposed by Hyland, et al. This method of impact mitigation is valid only when the uncertainty and modeling produce precise predictions for NGPs. However, the AEMP mission's scientific mission is increasingly necessary to produce these precise predictions.

In conclusion, the technique proposed by Hyland, et al should be further investigated. More research and observation is required to reduce uncertainty in the physical properties of Apophis and to refine NGP modeling. The expected radar observations in 2013 and potential follow-on exploration missions will do much to reduce these uncertainties and provide more data for analyzing future situations.

REFERENCES

Abe S., Mukai T., Hirata N., Barnouin-Jha O. S., Cheng A. F., Demura H., Gaskell R. W., Hashimoto T., Hiraoka K., Honda T., Kubota T., Matsuoka M., Mizuno T., Nakamura R., Scheeres D. J., Yoshikawa M.. 2006. Mass and local topography measurements of Itokawa by Hayabusa. Science 312, 1344-1347.

Alvarez L. W., Alvarez W., Asaro F., Michel H. V.. 1980. Extraterrestrial cause for the Cretaceous Tertiary extinction. Science 208, 1095-1099.

Barringer D. M.. 1905. Coon mountain and its crater." Proceedings of the Academy of Natural Sciences of Philadelphia, Vol. 57, 861-886.

Battin R. H.. 1999. An Introduction to the Mathematics and Methods of Astrodynamic, Revised Edition. AIAA Education Series, Reston, VA.

Behrend R.. 2004. Light curves of Apophis 99942. <http://obswww.unige.ch/~behrend/r099942a.png>. Retrieved Oct 2009.

Binzel R., Rivkin A. S., Thomas C. A., Vernazza P., Burbine T. H., DeMeo F. E., Bus S. J., Tokunaga A. T., Birlan M.. 2009. Spectral properties and composition of potentially hazardous Asteroid (99942) Apophis. Icarus 200, 480-485.

Bottke W., Vokrouhlický D., Rubincam D., Nesvorný D.. 2006. The Yarkovsky and YORP effects: Implications for asteroid dynamics. Annu. Rev. Earth Planet. Sci. 34, 157–191.

Bowell E., Hapke B., Domingue D., Lumme K., Peltoniemi J., Harris A.W.. 1989. Application of photometric models to asteroids. In: Binzel R. P., Gehrels T., Matthews M. S., Eds.): Asteroids II. University of Arizona Press, Tucson, 524–556.

Burns J., Lamy P., Soter S.. 1979. Radiation forces on small particles in the solar system. Icarus 40, 1-48.

Carusi A., Valsecchi G. B., Greenberg R.. 1990. Planetary close encounters: Geometry of approach and post-encounter orbital parameters. Cel. Mech. Dynam. Astron. 49, 111–131.

Chesley S., Milani A., Tholen D., Bernardi F., Chodas P., and Micheli M.. 2009. An updated assessment of the impact threat from 99942 Apophis. American Astronomical Society, DPS Meeting #41, #43.06. October 4-9, 2009, Fajardo, Puerto Rico.

Chesley S., Ostro S., Vokrouhlicky D., Capek D., Giorgini J.. 2003. Direct detection of the Yarkovsky effect by radar ranging to asteroid 6489 Golevka. Science 302, 1739–42

Delbò M., Cellino A., Tedesco E. F.. 2007. Albedo and size determination of potentially hazardous asteroids: (99942) Apophis. Icarus 188, 266-269.

Engineering Toolbox. Plastic Properties. <http://www.engineeringtoolbox.com>. Retrieved 10 Feb 2010.

Farinella P., Vokrouhlicky D.. 1999. Semimajor axis mobility of asteroidal fragments. Science 283, 1507–10.

Fujiwara A**.,** Kawaguchi J., Yeomans D. K., Abe M., Mukai T., Okada T., Saito J., Yano H., Yoshikawa M., Scheeres D. J., Barnouin-Jha O., Cheng A. F., Demura H., Gaskell R. W., Hirata N., Ikeda H., Kominato T., Miyamoto H., Nakamura A. M., Nakamura R., Sasaki S., Uesugi K.. 2006. The rubble-pile asteroid Itokawa as observed by Hayabusa. Science 312, 1330-1334.

Ghosh A., McSween H.. 1999. Temperature dependence of specific heat capacity and its effect on asteroid thermal models. Meteoritics & Planet. Sci., 34, 121–127.

Giorgini J., Benner A., Ostro S., Nolan M., Busch M.. 2008. Predicting the Earth encounters of (99942) Apophis. Icarus 193, 1-19.

Hyland D. C., Altwaijary H., Margulieux R.. 2009. A mission template for exploration and mitigation of potentially hazardous near Earth asteroids. International Symposium on Near-Earth Hazardous Asteroids, Valletta, Malta, October 9-11, 2009.

Hyland D. C., Altwaijary H., Margulieux R . 2009. A permanantly-acting NEA mitigation technique via the Yarkovsky effect. International Symposium on Near-Earth Hazardous Asteroids, Valletta, Malta, October 9-11, 2009.

Hyland D. C., Margulieux R., Young B., Sandberg J., Ge S.. 2010. “Apophis mitigation technology demonstration proposal.” Unpublished.

Japanese Aerospace Exploration Agency. 2010. Hayabusa project science database. <http://hayabusa.sci.isas.jaxa.jp>. Retrieved 24 Feb 2010.

Japanese Aerospace Exploration Agency. 2005. Hayabusa's scientific and engineering achievements during proximity operations around Itokawa. <http://www.isas.jaxa.jp/e/snews/2005/1102.shtml >. Retrieved 22 Feb 2010.

JPL Horizons. 2010. Earth Ephemeris. <http://ssd.jpl.nasa.gov/horizons.cgi>. Retrieved Jan 2010.

JPL Near Earth Object Program. 2010. Potentially hazardous asteroids. <http://neo.jpl.nasa.gov/neo/pha.html>. Retrieved Jan 2010.

JPL Small-Body Database. 2010. 99942 Apophis (2004 MN4). <http://ssd.jpl.nasa.gov/sbdb.cgi?sstr=99942>. Retrieved Jan 2010.

Kriens B. J., Shoemaker E. M., Herkenhoff K. E.. 1999. Geology of the Upheaval Dome impact structure, southeast Utah. J. Geophys. Res., 104, 18867–87.

La Spina A., Paolicchi P., Kryszczinska A., Pravec P.. 2004. Retrograde spins of near-Earth asteroids from the Yarkovsky effect. Nature 428, 400–1.

Lee P.. 1996. Dust levitation on asteroids. Icarus 124, 181-194.

Masuda H, Komatsu T., Iinoya K.. 1976. The static electrification of particles in gas-solids pipe flow. American Institute of Chemical Engineers Journal 22, 558-564.

Morbidelli A., Bottke W. F., Froeschle C., Michel P.. 2002. Origin and evolution of near-Earth objects. In: Bottke, W.F., Cellino, A., Paolicchi, P., Binzel, R.P.. Asteroids III, University of Arizona Press, Tucson, AZ, 409–422.

Müller T. G., Lagerros J. S. V.. 1999. Fundamental properties and thermophysical modelling of asteroids after ISO. American Astronomical Society, DPS meeting #31, #04.05, Padua, Italy October 1-5, 1999.

Opïk E. J.. 1976. Interplanetary encounters: Close-range gravitational interactions. Developments in Solar System and Space Science 2, 1-160.

Ostro S. J.. 1999. Asteroid 4179 Toutatis: 1996 radar observations. Icarus 137, 122–139.

Ostro S. J., Jurgens R. F., Rosema K. D., Hudson R. S., Giorgini J. D., Winkler R., Yeomans D. K., Choate D., Rose R., Slade M. A., Howard S. D., Scheeres D. J., Mitchell D. L.. 1996. Radar observations of asteroid 1620 Geographos. Icarus 121, 44–66.

Pelizzari M., Criswell D. R.. 1978. Lunar dust transport by photoelectric charging at sunset. Proc. Lunar Planet. Sci. Conf. 9, Houston, TX, March 13-17, 1978, 3225–3237.

Robertson H. P.. 1937. Dynamical effects of radiation in the solar system. Monthly Notices of the Royal Astronomical Society 97, 423-424.

Stuart J. S.. 2001. “A near-Earth asteroid population estimate from the LINEAR survey.” Science 294, 1691–1693.

Tholen D., Micheli M., Elliot G. T., Bernardi F.. Here is Apophis!. American Astronomical Society, DPS Meeting #41, #43.05. October 4-9, 2009, Fajardo, Puerto Rico.

Valsecchi G., Milani A., Gronchi G., Chesley S.. 2003. Resonant return to close approach: Analytical theory. Astron. Astrophys. 408, 1179-1196.

Vokrouhlicky D.. 1998. Diurnal Yarkovsky effect as a source of mobility of meter sized asteroidal fragments. I. Linear theory. Astron. Astrophys. 335, 1093–100.

Vokrouhlický D., Milani A., and Chesley S.. 2000. Yarkovsky effect on small near-Earth asteroids: Mathematical formulation and examples. Icarus, 148, 118–138.

Wertz J., Larson W.. 1999. Space Mission Analysis and Design, 3rd Edition. Microcosm Press, Hawthorne, CA.

Whipple E. C.. 1981. Potentials of Surfaces in Space. Rep. Prog. Phys. 44, 1197-1250.

Yeomans D., Chesley S., Chodas P.. 2004. Near-Earth asteroid 2004 MN4 reaches highest score to date on hazard scale. < http://neo.jpl.nasa.gov/news/news146.html>. Retrieved 12 Jan 2010.

APPENDIX A

EARTH EPHEMERIS

Orbital Element	**Value**
Eccentricity	0.0166366
Semi-major axis (AU)	1.00085
Time of last perihelion (JD)	2455202.90448
Longitude of the ascending node (deg)	178.577
Argument of the perihelion (deg)	287.163
Inclination (deg)	0.00396625

Retrieved from JPL Horizons Jan 2010.

APPENDIX B

APOPHIS COVARIANCE

	e	**q**	**t_p**	**node**	**peri**	**i**
e	1.306497E-15	-1.404556E-15	-7.757192E-14	1.246288E-13	-7.434097E-14	-8.170826E-15
q	1.404556E-15	1.522444E-15	8.928695E-14	-1.368158E-13	7.755698E-14	8.456046E-15
t_p	-7.757192E-14	8.928695E-14	5.107115E-11	-2.263577E-11	5.143169E-11	2.852090E-12
node	1.246288E-13	-1.368158E-13	-2.263577E-11	9.122141E-10	-9.156589E-10	-7.229408E-12
peri	7.434097E-14	7.755698E-14	5.143169E-11	-9.156589E-10	9.503140E-10	9.705785E-12
i	8.170826E-15	8.456046E-15	2.852090E-12 -	7.229408E-12	9.705785E-12	2.270877E-12

APPENDIX C

NGPs FOR UNMODIFIED LIMITING AND NOMINAL CASES

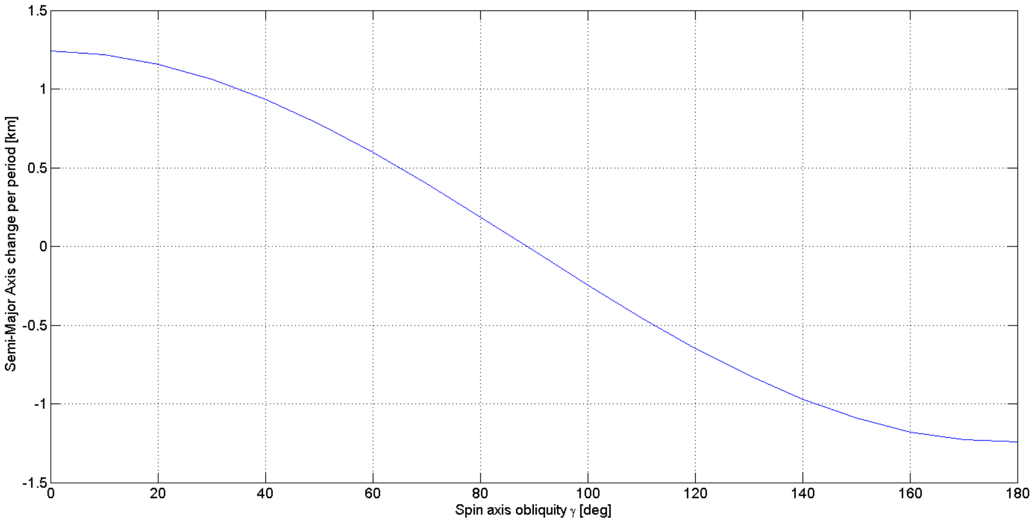

Most massive case variation in spin axis

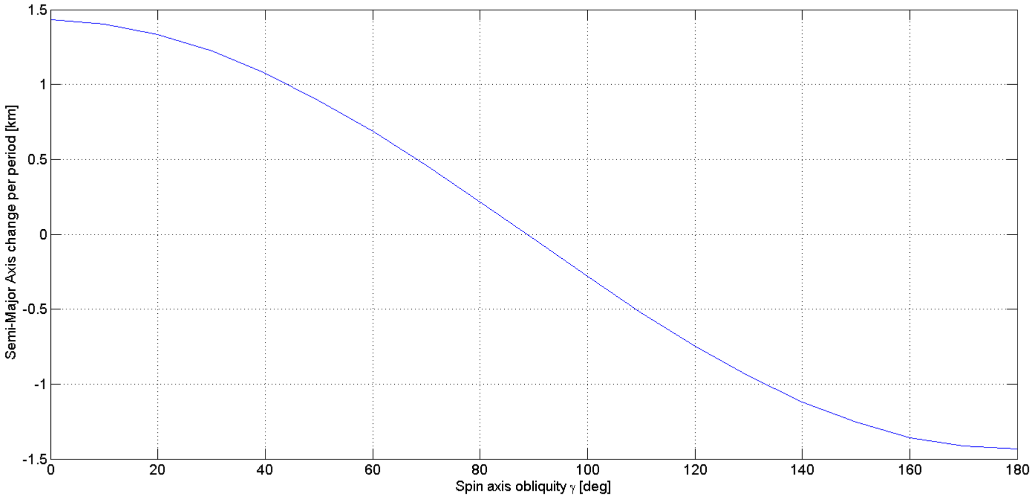

Least massive case variation in spin axis

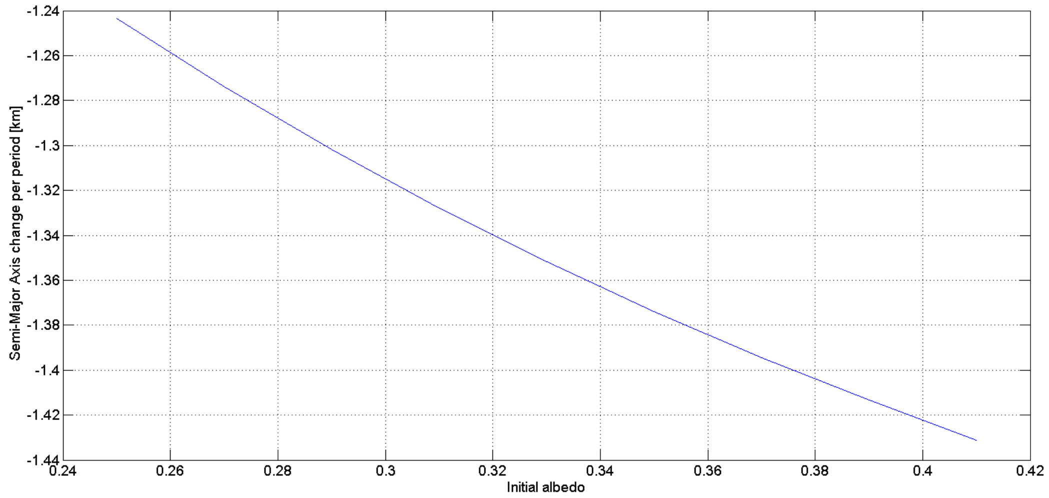

Retrograde spin variation in albedo

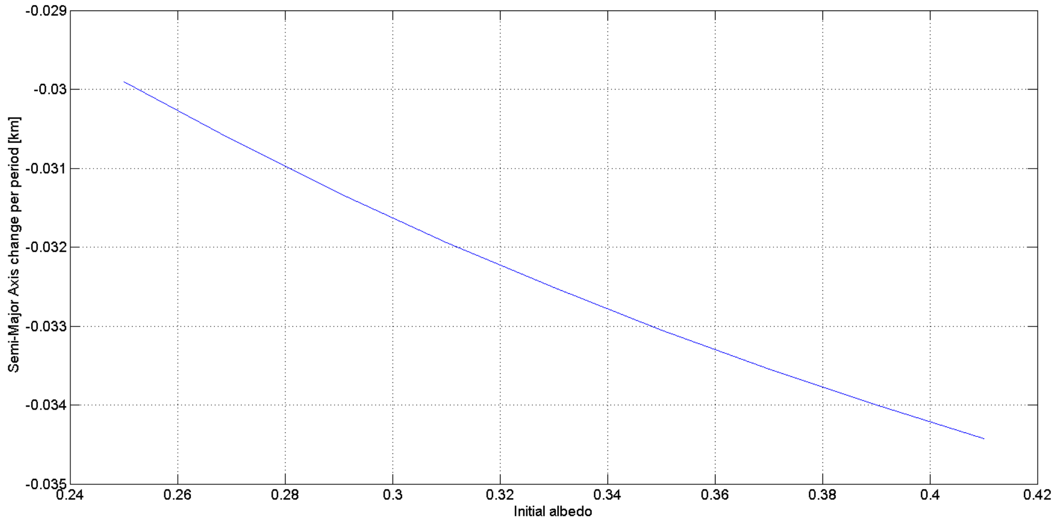

In-plane spin variation in albedo

APPENDIX D

KEYHOLE POS. RELATIVE TO ADJUSTED NOM. SOLUTION

*All distances are in km.

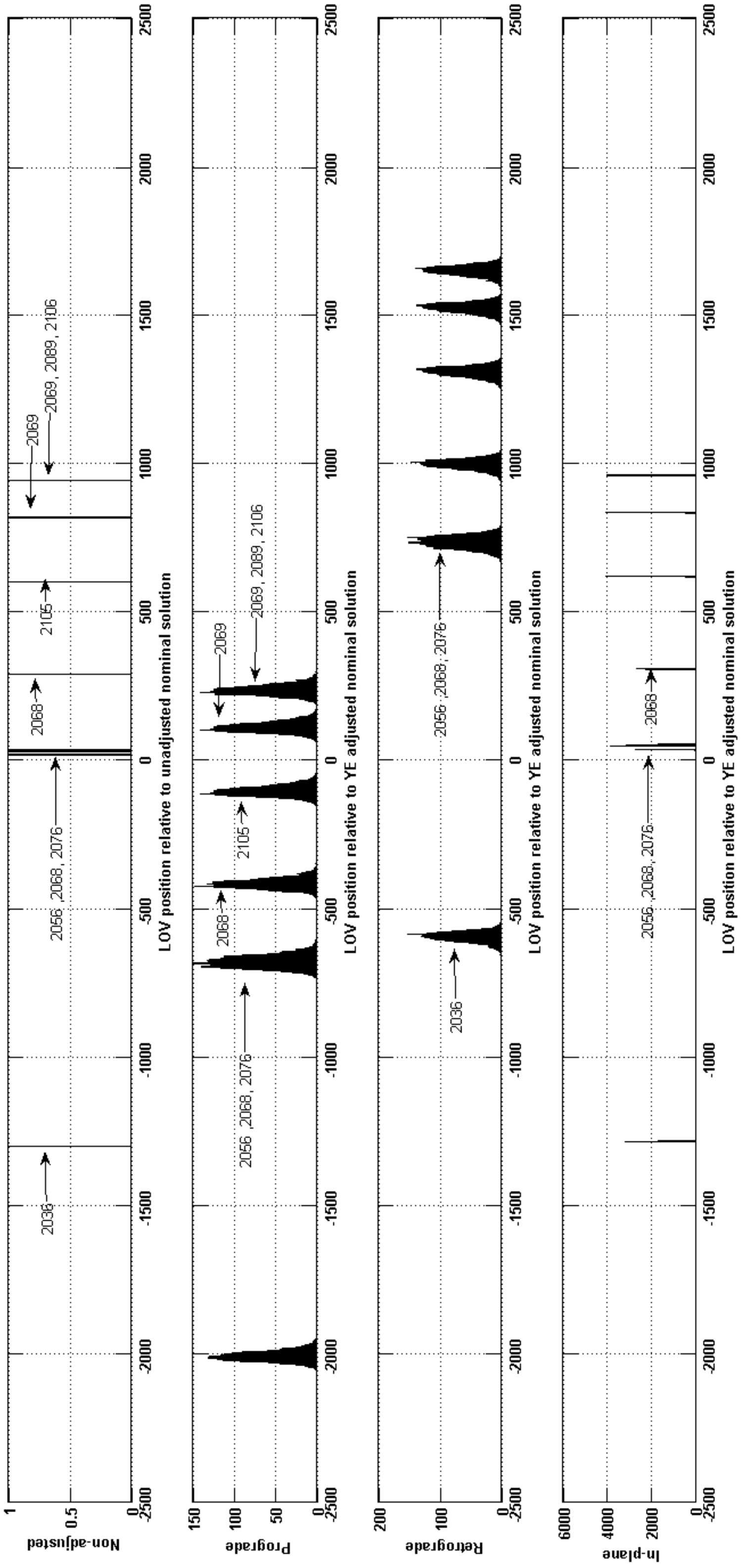

APPENDIX E

AEMP MISSION CONCEPT

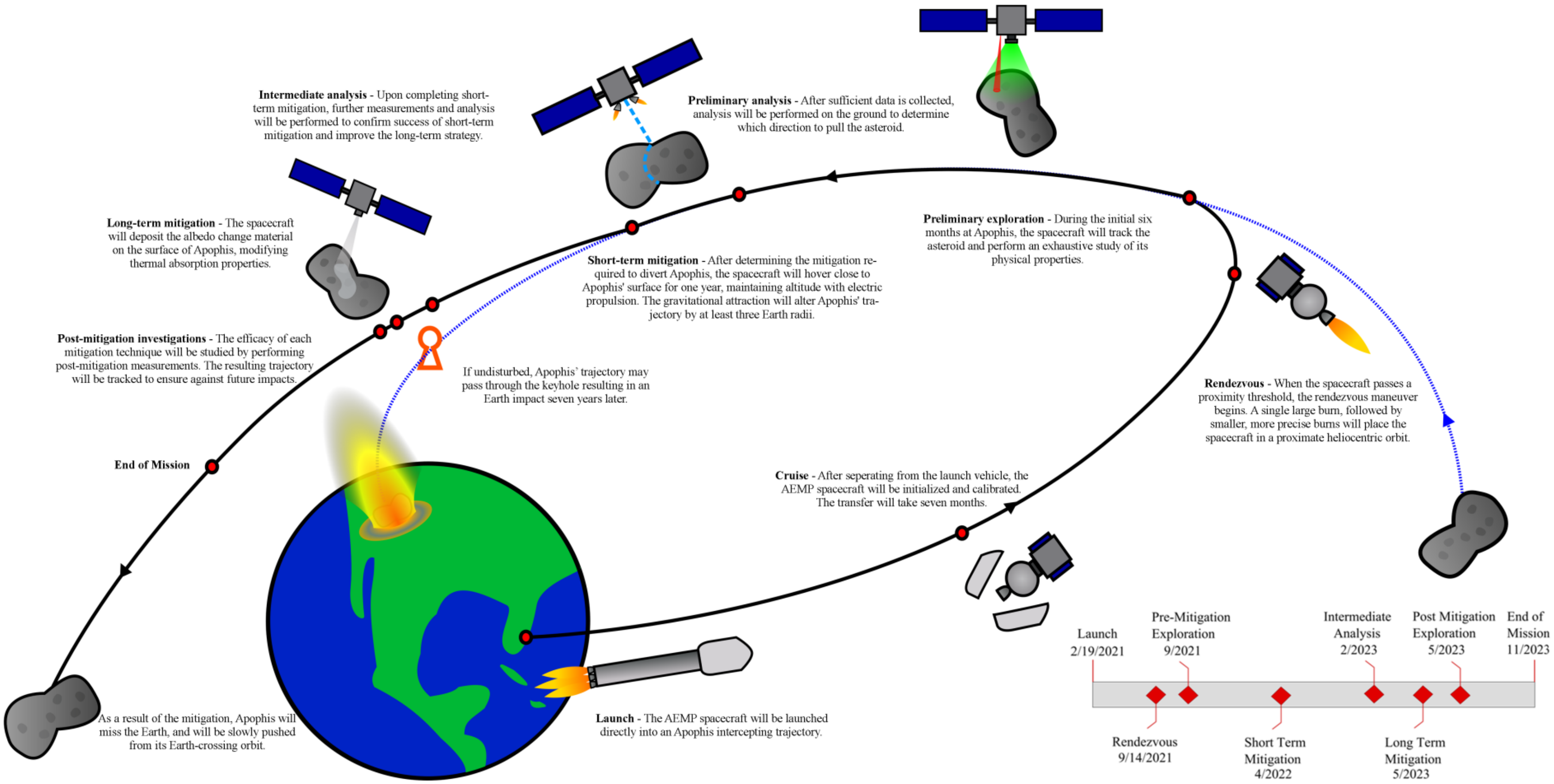

Intermediate analysis - Upon completing short-term mitigation, further measurements and analysis will be performed to confirm success of short-term mitigation and improve the long-term strategy.

Preliminary analysis - After sufficient data is collected, analysis will be performed on the ground to determine which direction to pull the asteroid.

Long-term mitigation - The spacecraft will deposit the albedo change material on the surface of Apophis, modifying thermal absorption properties.

Preliminary exploration - During the initial six months at Apophis, the spacecraft will track the asteroid and perform an exhaustive study of its physical properties.

Short-term mitigation - After determining the mitigation required to divert Apophis, the spacecraft will hover close to Apophis' surface for one year, maintaining altitude with electric propulsion. The gravitational attraction will alter Apophis' trajectory by at least three Earth radii.

Post-mitigation investigations - The efficacy of each mitigation technique will be studied by performing post-mitigation measurements. The resulting trajectory will be tracked to ensure against future impacts.

If undisturbed, Apophis' trajectory may pass through the keyhole resulting in an Earth impact seven years later.

Rendezvous - When the spacecraft passes a proximity threshold, the rendezvous maneuver begins. A single large burn, followed by smaller, more precise burns will place the spacecraft in a proximate heliocentric orbit.

End of Mission

Cruise - After seperating from the launch vehicle, the AEMP spacecraft will be initialized and calibrated. The transfer will take seven months.

Launch - The AEMP spacecraft will be launched directly into an Apophis intercepting trajectory.

As a result of the mitigation, Apophis will miss the Earth, and will be slowly pushed from its Earth-crossing orbit.

VITA

Name: Richard Steven Margulieux

Address: Richard Margulieux
Texas A&M University
Department of Aerospace Engineering
701 HR Bright Building
College Station, TX 77843-3141

Email address: rmargulieux@gmail.com

Education: B.S. Aerospace Engineering, Texas A&M University, 2008

M.S. Aerospace Engineering, Texas A&M University, 2010